

BREAKING COSMOLOGICAL DEGENERACIES IN GALAXY CLUSTER SURVEYS WITH A PHYSICAL MODEL OF CLUSTER STRUCTURE

JOSHUA D. YOUNGER¹, ZOLTÁN HAIMAN², GREG L. BRYAN², AND SHENG WANG^{3,4}

¹Columbia Astrophysics Lab, Columbia University, Pupin Physics Laboratories, New York, NY 10027

²Department of Astronomy & Astrophysics, Columbia University, Pupin Physics Laboratories, New York, NY 10027

³Department of Physics, Columbia University, Pupin Physics Laboratories, New York, NY 10027 and

⁴Brookhaven National Laboratory, Upton, NY 11973-5000

Draft version October 10, 2018

ABSTRACT

It has been shown that in an idealized galaxy cluster survey, containing $\gtrsim 10,000$ clusters, statistical errors on dark energy and other cosmological parameters will be at the percent level. Furthermore, through “self-calibration”, parameters describing the mass-observable relation and cosmology can be simultaneously determined, though at a loss in accuracy by about an order of magnitude. Here we examine an alternative approach to self-calibration, in which a parametrized ab-initio physical model is used to compute theoretical mass-observable relations from the cluster structure. As an example, we use a modified-entropy (“preheating”) model of the intracluster medium, with the history and magnitude of entropy injection as unknown input parameters. Using a Fisher matrix approach, we evaluate the expected simultaneous statistical errors on cosmological and cluster model parameters. We find that compared to a phenomenological parametrization of the mass-observable relation, our physical model yields significantly tighter constraints in both surveys, and offers substantially improved synergy when the two surveys are combined. In a mock X-ray survey, we find statistical errors on the dark energy equation of state are a factor of two tighter than the phenomenological model, with $\Delta w_0 \sim 0.08$ and its evolution, $\Delta w_a \equiv -\Delta dw/da \sim 0.23$, with corresponding errors of $\Delta w_0 \sim 0.06$ and $\Delta w_a \sim 0.17$ from a mock Sunyaev-Zel’dovich (SZ) survey, both with $N_{cl} \sim 2.2 \times 10^4$ clusters, while simultaneously constraining cluster model parameters to $\lesssim 10\%$. When the two surveys are combined, the constraints tighten to $\Delta w_0 \sim 0.03$ and $\Delta w_a \sim 0.1$; a 40% improvement over adding the individual experiment errors in quadrature, and a factor of 2 improvement over the phenomenological model. This suggests that parametrized physical models of cluster structure will be useful when extracting cosmological constraints from SZ and X-ray cluster surveys.

Subject headings: cosmology:observations-cosmology:theory-cosmological parameters-dark matter-galaxies:clusters:general-large-scale structure of the universe

1. INTRODUCTION

It has been known for about two decades that clusters of galaxies provide a uniquely powerful probe of fundamental cosmological parameters. As the most massive virialized objects in the universe, they form at the highest peaks in the primordial density field, and as a result, their abundance and spatial distribution are very sensitive to the underlying cosmology (e.g., Bahcall 1988; Peebles 1993; Carlberg et al. 1997; Rosati et al. 2002; Henry 2004). Strong constraints have already been derived on the present day matter density Ω_m , and the normalization of the dark matter power spectrum σ_8 (Peebles, Daly, & Juszkwicz 1989; Henry & Arnaud 1991; Bahcall & Cen 1992; Viana & Liddle 1996; Bahcall & Bode 2003; Bahcall et al. 2003), using only dozens of clusters. In large future surveys, with tens of thousands of clusters, high-precision constraints are expected to be available on dark energy parameters (Haiman, Mohr, & Holder 2001), including constraints on the evolution of the equation of state $w_a \equiv dw/da$ (Weller, Battye, & Kneissl 2002; Weller & Battye 2003; Wang et al. 2004).

Plans are currently being drafted for the first very large scale clusters surveys. These projects, such as the 4,000 degree² South Pole Telescope that will find clusters through the SZ effect (hereafter SPT; Ruhl et al. 2003),

a proposed larger X-ray survey (Haiman et al. 2005), or catalogs of clusters identified in wide weak-lensing surveys, such as LSST (Tyson 2002), promise to produce catalogs of many thousands of clusters, containing a rich resource of cosmological information. With such an increase in the data looming on the horizon, it is becoming increasingly important to understand the inherent systematics, and establish realistic expectations for potential cosmological constraints.

Several recent works, motivated by the above considerations, have focused on various aspects of extracting cosmological parameters from high-yield future surveys, such as the statistical constraints available on curvature Ω_k (Holder, Haiman, & Mohr 2001), assessing the impact of sample variance (Hu & Kravtsov 2003) and other uncertainties (Levine, Schultz, & White 2002) on parameter estimates, and controlling such uncertainties by utilizing information from the shape of the cluster mass function dN/dM (Hu 2003). Recent studies have also elucidated the additional cosmological information available from the spatial distribution of galaxy clusters through a measurement of their three-dimensional power spectrum (Hu & Haiman 2003), utilizing both the intrinsic shape of the transfer function (Refregier, Valtchanov, & Pierre 2002) and baryon features (Blake & Glazebrook 2003; Seo & Eisenstein

2003; Linder 2003).

Most importantly, recent work has focused on the systematic errors on cosmological parameters arising from the inherent uncertainties on the mass–observable relation. It has been shown that large forthcoming cluster surveys can be “self-calibrating”, in the sense that when the abundance and clustering properties of clusters are considered in tandem, tight constraints can be derived on cosmology even if the mass–observable relation has to be determined simultaneously from the same data (Majumdar & Mohr 2004; Wang et al. 2004; Lima & Hu 2005). In these studies, the mass–observable relation was assumed to be either unknown a priori, or to have a simple parametric form (such as a power-law).

While these assumptions have been demonstrated to yield interesting constraints, one may argue that this approach is overly conservative. In particular, it is reasonable to expect that the structure of clusters, such as their mean density and temperature profiles, can be at least approximately computed from ab-initio models. The simplest, spherically symmetric, self-similar models contradict observations, such as the relation between X-ray flux (L_x) and temperature (T), or the resolved profiles of low-mass clusters (Voit et al. 2002). However, motivated by the observations of Ponman et al. (1999), modified-entropy models of the intra-cluster medium (ICM), while still not correct in detail (Pratt & Arnaud 2005; Pratt, Arnaud, & Pointecouteau 2006; Younger & Bryan 2006), have been successful at predicting the mass–observable scalings in temperature, luminosity, and SZ effect, from first principles (Voit et al. 2002; McCarthy et al. 2003a,b). It is reasonable to expect that our understanding of the physics determining the structure of clusters will be improved in the future by advances in both observations and numerical simulations.

In this paper, we study the utility of a partial understanding of the ICM in improving cosmological constraints. We will show that using a-priori cluster structure models, it is possible to significantly improve cosmological constraints, relative to direct, phenomenological self-calibration of the mass–observable relation – even if the physical model has free parameters. Furthermore, the combination of X-ray and SZ datasets is particularly promising (Verde, Haiman, & Spergel 2002), and can more effectively break degeneracies, since the underlying models directly relate the SZ decrement to the X-ray flux. The end result is significantly improved errors on the cosmology, using the same observational data set, in addition to a well constrained model of the ICM.

The rest of this paper is organized as follows. In §2, we describe our models of cluster structure and evolution in the presence of a preheating of the ICM gas. In §3, we discuss our fiducial model, and demonstrate that it satisfies a number of existing observations. In §4, we contrast our physical models with a “traditional” conservative approach to self-calibration, in which the mass–observable relation is parametrized directly as a power-law. In §5, we discuss and motivate the parameters of our mock cluster surveys, and, for comparison, discuss future measurements of cosmic microwave background (CMB) anisotropies. In §6, we briefly summarize the Fisher matrix approach, as applied to cluster surveys and CMB anisotropies. In §7, we present and crit-

ically discuss our results, by comparing the constraints obtained under self-calibration and under the assumption of physical cluster models. Finally, in §10, we summarize our main conclusions and the implications of this work.

2. CLUSTER STRUCTURE AND EVOLUTION MODELS

In this section, for completeness and specificity, we describe our models for the structure – density and temperature profiles – of galaxy clusters, in the presence or absence of excess entropy. Our treatment assumes that the gas is in hydrostatic equilibrium in a dark matter (DM) potential, and it closely follows previous studies on cluster profiles and preheating.

2.1. Motivation

Modified entropy models are physically motivated by the presence of a universal entropy floor. Ponman et al. (1999) find that the entropy distribution of ICM gas, as inferred from ROSAT observations of 25 galaxy clusters, is inconsistent with simple gravitational collapse, and suggest instead the presence of an entropy floor of $K_0 \sim 100h^{-1/3}$ keV cm². This excess entropy is itself potentially a relic of winds and outflows from galaxies that formed in the protocluster, and heated the ICM at moderate redshift $z \sim 2$, prior to cluster collapse. They then argue that this results in the observed departure of real galaxy clusters from the expected self-similar scaling. However, it is plausible that only a fraction of this preheating entropy is injected at high redshift. Some of the heat input may come from a combination of active galactic nuclei (AGN) and supernovae (SN), over an extended period, rather than winds in a narrow redshift range. For this reason, it is useful to treat K_0 as a function of redshift, which can be parametrized, for example, by a power-law relation $K_0(z) = K_0(z=0)(1+z)^{\alpha_K}$.

We assume that clusters at a given redshift z are spherically symmetric and in hydrostatic equilibrium, with an ideal gas ICM consisting of a fully ionized H–He plasma with the cosmic helium mass fraction $Y_{\text{He}} = 0.25$, and a mean molecular weight $\mu = 0.59$. The unmodified entropy distribution is constructed by assuming that the gas traces the dark matter (DM), and that the total gas density is given by a fraction f_g of the cosmological baryon density within the virialized cluster that remains in the ICM. The DM and gas profile is assumed to follow the Navarro, Frenk & White (1997) (NFW) form, as motivated by N-Body simulations, with a fixed concentration parameter $c = 5$ (Eke, Navarro, & Steinmetz 2001). The assumption of hydrostatic equilibrium, together with physically motivated boundary conditions, allows us to calculate the pressure and temperature profiles, which, combined with the gas density, give the entropy distribution as a function of radius. This entropy distribution is then modified by adding a constant K_0 at all radii, and the hydrostatic equilibrium equations are re-integrated under the assumption that mass shells do not cross (i.e. $K(M_g)$ is conserved where M_g is the total gas mass at that radius). The resulting modified density and temperature profiles have flat cores, and they can be used to predict cluster observables, such as the X-ray flux or SZ decrement.

2.2. Unmodified Equilibrium Structure

The ICM is assumed to trace the DM, which is well-described by an NFW profile of the form

$$\rho_{DM}(r) = \frac{\delta_c \rho_c}{(r/R_s)(1+r/R_s)^2} \quad (1)$$

where R_s is a scale radius defined in terms of the concentration parameters c and the virial radius, as in Bullock et al. (2001), by

$$cR_s = R_v = \left(\frac{3M}{4\pi\Delta_v\rho_c} \right)^{1/3} \quad (2)$$

and

$$\delta_c = \frac{\Delta_v}{3} \frac{c^3}{\ln(1+c) - \frac{c}{1+c}}. \quad (3)$$

In both cases Δ_v is the virial overdensity relative to the critical density of the universe ρ_c given as a fitting form for a flat universe by Kuhlen et al. (2005), extended to include a time-evolving dark energy:

$$\Delta_v = 18\pi^2\Omega_m(z)[1 + a\Theta^b(z)] \quad (4)$$

where $\Theta(z) = \Omega_m^{-1}(z) - 1$, $\Omega_m(z)$ is the matter density of the universe as a function of redshift z , $a = 0.432 - 2.001(|w(z)|^{0.234} - 1)$, $b = 0.929 - 0.222(|w(z)|^{0.727} - 1)$, and w comes from the dark energy equation of state $w = w_0 + w_a \frac{z}{1+z}$ (Chevallier & Polarski 2001; Linder 2003). The gas is assumed to trace the DM distribution for a given cosmology with a constant gas fraction $f_g \sim 0.8$,

$$\rho_g(r) = \frac{\delta_c \rho_c}{(r/R_s)(1+r/R_s)^2} f_g f_b \quad (5)$$

where $f_b = \Omega_b/\Omega_m$ is the mean baryon fraction of the universe.

The corresponding ICM pressure and temperature profiles are computed by integrating the equations of hydrostatic equilibrium and mass conservation for an ideal gas,

$$\frac{dP}{dr} = \rho_g g(r) \quad (6)$$

$$\frac{dM_g}{dr} = 4\pi r^2 \rho_g \quad (7)$$

$$P = nk_B T = \frac{\rho_g k_B T}{\mu m_p} \quad (8)$$

where k_B is the Boltzmann constant, m_p is the mass of a proton, $\mu = 0.59$ is the mean molecular weight, and

$$g(r) = -\frac{G(M_{DM} + M_g)}{r^2} \quad (9)$$

is the gravitational acceleration including the self-gravity of the gas. Once $P(r)$ and $T(r)$ are determined, the entropy profile $K(r)$ is computed according to

$$K = Tn^{-2/3} \quad (10)$$

where n is the total gas¹ particle number density $n = P/k_B T$. The outer boundary condition is taken to be a pressure resisting the infall of baryonic matter at the virial radius; $P_{vir} = f_b \rho_{DM} v_{ff}^2/3$, with v_{ff} the free-fall velocity at the virial radius as in Voit et al. (2002).

¹ This in contrast to typical observational definitions which use the electron density n_e

2.3. The Modified Distribution

After the unmodified entropy distribution has been calculated, we follow Voit et al. (2002), and increase it by a constant K_0 as

$$\hat{K}(r) = K(r) + K_0 \quad (11)$$

where $K(r)$ is the unmodified distribution and K_0 is a constant of order 100 keV cm², assumed here to evolve with redshift as $K_0 = K_0(z=0)(1+z)^{\alpha_K}$. This mimics the preheating of the ICM, whereby some mechanism had injected a fixed amount of entropy into the gas prior to its collapse at redshift z (Ponman et al. 1999; Voit et al. 2002).

We change variables and re-integrate the equations of hydrostatic equilibrium using the modified entropy distribution \hat{K} . The equation of hydrostatic equilibrium then reads

$$\frac{dP}{dr} = g(r)\rho_g(P, \hat{K}) \quad (12)$$

where, casting the pressure and temperature in terms of P and \hat{K}

$$\rho_g = \mu m_p \left[\frac{P}{k_B \hat{K}(M_g)} \right]^{3/5}. \quad (13)$$

and

$$k_B T = \hat{K}(M_g)^{3/5} P^{2/5} \quad (14)$$

We use the same pressure matching boundary condition as before. This procedure results in modified profiles for P , ρ_g , and T that can be used to make predictions for different bulk properties of the cluster, and to establish the expected mass-observable relations.

2.4. Radial Profiles

Before considering the effects of entropy modification on the bulk properties of the ICM, it is instructive to visualize its impact on the radial profiles of clusters of different masses. In particular, for reference, we examine the effects of entropy modifications with $K_0 = 50$ and 100 keV cm² as compared to the unmodified model on two clusters with $M_{vir} = 10^{14}$ and $10^{15} h^{-1} M_\odot$ respectively, at redshift $z = 0$, with our fiducial Λ CDM cosmology (see definition below). The radial temperature, pressure, and gas density (T, P, ρ_g) profiles are plotted in Figure 1.

The overall impact of the entropy injection is to depress and flatten the core pressure and density. This results in a flattened inner gas density profile (Sun et al. 2003; Pointecouteau et al. 2004) and an outer ($r > 0.1R_v$) temperature profile (Vikhlinin et al. 2004), resembling the results of recent X-ray observations. It is important to note that the effects of preheating are more pronounced for a low mass cluster than for a high mass cluster, with the limit that at very high mass the entropy injection becomes unimportant. This is because the injection is a decreasing percentage of the unmodified entropy at a given radius as the cluster mass increases.

2.5. Observables

In order to judge the fitness of our model for use in later cosmological measurements, we first need to confirm that it can reproduce the observed scalings for the $M - T$ and $L_x - T$ relations, given the right choices for the

input parameters f_g and K_0 . We recall that the X-ray luminosity scales approximately as $L \propto \rho_g^2$, and define the luminosity weighted temperature as

$$T_{\text{lum}} = \left(\int \rho_g^2(r) T(r) dV \right) \left(\int \rho_g^2(r) dV \right)^{-1} \quad (15)$$

where the integrations (as in all the following cases) are performed over the entire volume of the cluster out to the virial radius $r = R_v$.

We then assume a fully ionized H–He plasma with a hydrogen mass fraction $X = 0.75$, $n_e = \rho_g \left(\frac{X}{m_p} + \frac{1-X}{2m_p} \right)$ and $n_H = \rho_g \frac{X}{m_p}$, and calculate the X-ray luminosity as

$$L_x = \int \int n_e n_H \Lambda_\nu(T) dV d\nu. \quad (16)$$

Here $\Lambda_\nu(T)$ is the Raymond & Smith (1977) cooling function for a gas of metallicity $Z = 0.3Z_\odot$ for either the bolometric or the K-corrected soft X-ray emissivity in the 0.5 – 2.0 keV band.

Inverse Compton scattering by electrons in the hot ICM manifests itself as a fractional change in the temperature of the Cosmic Microwave Background (CMB), which at frequencies less than $\nu \sim 218$ GHz appears as a decrement (Sunyaev & Zeldovich 1972, 1980). This effect, often referred to as the thermal SZ effect, provides a useful probe of the electron pressure P_e integrated along the line-of-sight (assuming the electrons and gas are in thermal equilibrium), which complements the X-ray luminosity measurements. We calculate both the central and integrated SZ flux according to the prescription in McCarthy et al. (2003a,b).

The amplitude of the SZ effect is encoded in the Compton parameter,

$$y(\theta) = \frac{\sigma_T}{m_e c^2} \int P_e dl \quad (17)$$

where σ_T is the Thompson cross section and $P_e = n_e k_B T$ is the electron pressure integrated along the line of sight dl . The central decrement $y_0 = y(\theta = 0)$, and the SZ flux is

$$S_\nu = j_\nu(x) y_{\text{int}} \quad (18)$$

where $x = h\nu/k_B T_{\text{CMB}}$ with $T_{\text{CMB}} = 2.728$ (Fixsen et al. 1996) is the dimensionless frequency, $j_\nu(x) = 2(k_B T_{\text{CMB}})^3 (hc)^{-2} f_\nu(x)$ describes the spectrum of the SZ effect, and

$$y_{\text{int}}(\leq \theta) = 2\pi \int_0^\theta y(\theta') \theta' d\theta' \quad (19)$$

We choose our observable as the integrated SZ flux,

$$S_\nu = y_{\text{int}} \frac{2(k_B T_{\text{CMB}})^3}{(hc)^2} f_\nu, \quad (20)$$

evaluated at the frequency $\nu = 150$ GHz.

3. THE FIDUCIAL MODEL AND COSMOLOGY

In this section, we discuss the parameter choices in our fiducial model. Our aim is to demonstrate that our fiducial model is in rough agreement with a number of existing observations.

The observations we are mainly interested in matching are the scaling relations between cluster mass and observables, such as $M_{200} - L_{\text{bol}}$, $M_{500} - S_\nu/f_\nu$, and $L_{\text{bol}} - S_\nu/f_\nu$, where M_Δ represents the mass within a spherical overdensity of $\Delta\rho_c$. These relations drive the constraints we will derive below, and they have been estimated in observations over a range of redshifts. In comparisons to published data, we obtain the relevant cluster mass assuming an NFW profile with a concentration parameter $c = 5$. We find that the data suggest a non-evolving ($\alpha_K = 0$) entropy floor of $K_0 = 125h^{-1/3}$ keV cm² with a fixed gas fraction $f_g = 0.8$, which are roughly consistent with the observations of Ponman et al. (1999) and Lloyd-Davies, Ponman, & Cannon (2000).

In Figure 2, in the lower panel, we show the local $M_{200} - L_{\text{bol}}$ scaling relation found by Reiprich & Böhringer (2002) at $0 < z \lesssim 0.1$, along with the predictions from the unmodified model (dot-dashed curve) and from our fiducial model (solid curve) at $z = 0.05$. In the upper panel of the same figure, we show the observational data of Maughan et al. (2005) for the same scaling relation over the redshift range $0.7 < z < 0.9$, compared to our predictions for both the unmodified and the fiducial models at $z = 0.8$. In the model predictions in both panels, we adopt the same cosmology as used in the observational papers (different from our fiducial cosmology, discussed below). The plot shows good agreement between the data and our fiducial model over the full redshift range (and the unmodified self-similar model is clearly ruled out). The models also predict the ICM gas temperature, and as another check, in Figure 3 we compare these predictions to data on the local $T - M_{500}$ and $T - L_{\text{bol}}$ scalings from Reiprich & Böhringer (2002). Again, we find rough agreement between our predictions and the observed data, although the models slightly overpredict the temperatures of the lowest-mass clusters. We find that our models are also in good agreement with other determinations of both the local mass-temperature (White, Jones, & Forman 1997; Girardi et al. 1998; Finoguenov, Reiprich & Böhringer 2001; Sanderson et al. 2003) and temperature-luminosity (Markevich 1998; Arnaud & Evrard 1999; Fairley et al. 2000; Novicki, Sornig, & Henry 2002) relations.

The predictions of the fiducial model were then compared to measurements of the SZ decrement. In Figure 4, we show our model predictions at four different redshifts between $0.1 < z < 0.4$, for both the $M_{500} - S_{\text{arc},\nu}/f_\nu$ and $L_{\text{bol}} - S_{\text{arc},\nu}/f_\nu$ scalings, where $S_{\text{arc},\nu}/f_\nu$ is the frequency independent integrated SZ flux in a circle with radius 1 arc-second centered on the cluster. Also shown in the figure are the observational data from McCarthy et al. (2003b) and references therein, for the full redshift range $z \sim 0.1 - 0.4$. Again, we find good agreement between our fiducial model and the observed scalings involving the SZ decrement – although the data is still sparse, and shows a large scatter.

For the fiducial cosmology, we adopt $(\Omega_m h^2, \Omega_{DE}, w_0, w_a, \sigma_8, \Omega_b h^2, n_s) = (0.14, 0.73, -1.0, 0, 0.7, 0.024, 1.0)$. With the exception of σ_8 , these values are taken from the best-fit Λ CDM model found in the first-year *WMAP* data

(Spergel et al. 2003). It has been shown previously that the local cluster mass–temperature relation implies a lower value of σ_8 than CMB observations (Seljak 2002). We arrive at the same conclusion, when we adjust σ_8 such that the model predictions agree with the number counts of X-ray clusters. For the flux limit of $F_x(0.5 - 2.0 \text{ keV}) > 3 \times 10^{-14} \text{ erg s}^{-1} \text{ cm}^{-2}$ of the deepest existing X-ray surveys (Vikhlinin et al. 1998; Gioia et al. 2001; Rosati et al. 2002), which is also approximately the limiting flux proposed for a new all-sky survey (Haiman et al. 2005), we find that we need to set $\sigma_8 = 0.7$ in order to be consistent with the observed cumulative number counts (about 5.5 clusters/degree² for the above threshold; see Fig. 5). This low value of σ_8 is, in fact, consistent with the recent year–three *WMAP* results (Spergel et al. 2005), and also with previous estimates based on the local mass–temperature relation (Seljak 2002; Pierpaoli et al. 2003), galaxy velocity fields (Willick & Strauss 1998), and weak lensing measurements (Brown et al. 2002; Hoekstra et al. 2002; Jarvis et al. 2003). Our fiducial cosmology is also consistent with other cluster count measurements using optical (Bahcall et al. 2003) and X-ray selected samples (Borgani et al. 2001; Shuecker et al. 2003; Gladders et al. 2006).

Finally, despite its rough success, we call attention to potentially interesting tension between our fiducial model predictions and observations. In particular, for both the local and high redshift scaling relations shown in Figure 3, the cluster temperatures are somewhat overpredicted for the lowest mass clusters. Likewise, Figure 5 shows that our model $\log N - \log S$ relation somewhat overpredicts the number of bright clusters. That the current cluster data reveals such tension highlights the potential of larger surveys in calibrating models of the ICM simultaneously with cosmology. In the present paper, however, our goal is to explore a methodology, rather than a specific cluster model. We made use of the existing data only to guide us in choosing a reasonable set of fiducial parameters, and we postpone a more rigorous study of the viability of this model to future work.

4. THE PHENOMENOLOGICAL MODEL

Our aim in this paper is to quantify the merits of using a model for the cluster, as opposed to directly self-calibrating the mass–observable relation, as proposed in previous studies (Majumdar & Mohr 2004; Wang et al. 2004). The later approach will be hereafter referred to as a “Phenomenological Model.” To enable a comparison between the two approaches, we here consider joint cosmological and “cluster model” constraints, adopting simple parametric power–law scalings for the mass–observable relation to include the latter. We follow Majumdar & Mohr (2004) and Wang et al. (2004), and parametrize the X–ray luminosity as

$$L_{x,bol} = 4\pi F_x d_L^2 = A_x M_{200,15}^{\beta_x} E^2(z)(1+z)^{\gamma_x} \quad (21)$$

where d_L is the luminosity distance in Mpc, L_x is the bolometric X–ray luminosity in units of erg s^{-1} , F_x is the observed bolometric X–ray flux in units of $\text{erg s}^{-1} \text{ cm}^{-2}$, $M_{200,15}$ is the mass of the cluster within an overdensity of $200\rho_c$ in units of $10^{15} M_\odot$, with a normalization $\log A_x = -3.56$ (see §5.1 for details). We apply a

K–correction to obtain the flux in the 0.5–2.0 keV band, $L_x(0.5 - 2.0 \text{ keV}) = L_{x,bol} k(z)$, with

$$k(z) = \frac{\int_{\nu_1(1+z)}^{\nu_2(1+z)} \Lambda_\nu(T) d\nu}{\int_0^\infty \Lambda_\nu(T) d\nu}, \quad (22)$$

where $\Lambda_\nu(T)$ is the Raymond & Smith (1977) cooling function for a gas of metallicity $Z = 0.3Z_\odot$ and temperature T . The ICM gas temperature in the direct self-calibration case is needed only for this K-correction, and was estimated using the observed mass–temperature relation of Finoguenov, Reiprich & Böhringer (2001),

$$M_{180} = (1 \pm 0.2) \times 10^{15} h^{-1} M_\odot \left(\frac{T}{\beta_T \Delta_v^{1/3} \text{ keV}} \right)^{3/2} \quad (23)$$

where M_{180} is the cluster mass within an overdensity of 180 relative to the background, $\beta_T = 1.75 \pm 0.25$, and Δ_v is the virial overdensity.

The SZ flux is parametrized similarly as a power–law,

$$S_\nu d_A^2 = A_{sz} M_{200,15}^{\beta_{sz}} E^{2/3}(z)(1+z)^{\gamma_{sz}} \quad (24)$$

where d_A is the angular diameter distance in Mpc, and S_ν has units of mJy at a frequency of $\nu = 150 \text{ GHz}$, with a normalization $\log A_{sz} = 8.29$ (see §5.2 for details).

5. SIMULATING GALAXY CLUSTER SURVEYS

To simulate the abundance of clusters of galaxies, we begin with the standard formalism (Press & Schechter 1974),

$$\frac{dn}{d \ln M} = f(M) \frac{\rho_0}{M} \frac{d \log \sigma^{-1}}{d \ln M} \quad (25)$$

where M is measured out to an spherical overdensity of 180 relative to the background, ρ_0 is the present day background matter density, $f(M)$ is taken from the extended Press-Schechter fit of Jenkins et al. (2001), and σ is the variance of the linear density field at redshift z . The power spectrum was calculated using the fitting formulae of Eisenstein & Hu (1999), modified to include the effects of a time-varying dark energy parameter with $w(z) = w_0 + w_a \frac{z}{1+z}$ (Linder 2003).

The quantity we will use below to derive cosmological constraints is the number of clusters within a bin corresponding to a range of the observable Ψ . We follow Lima & Hu (2005) and include a constant log–normal scatter in the cluster mass at a fixed observable, with standard deviation $\sigma_{\log M|\Psi}$. In the absence of scatter, we use our mass–observable relation – either the phenomenological or physical model – to map the flux bin $\Psi_i < \Psi < \Psi_{i+1}$ to a mass bin $M_{obs}^i < M_{obs} < M_{obs}^{i+1}$, to compute the expected counts. In the presence of scatter, for a redshift bin centered at z_j of width Δz , the expected counts within $\Psi_i < \Psi < \Psi_{i+1}$ is modified to

$$N_i(z_j) = \Delta\Omega \Delta z \frac{dV}{dz d\Omega} \int \frac{d \ln M}{2} \frac{dn}{d \ln M} [\text{erfc}(x_i) - \text{erfc}(x_{i+1})] \quad (26)$$

where

$$x_i = \frac{\log M - \log M_{obs}^i}{\sqrt{2\sigma_{\log M|\Psi}^2}} \quad (27)$$

and $dV/dz d\Omega$ is the comoving volume element, and erfc is the complementary error function.

5.1. Survey Parameters

Our mock X-ray survey has a flux detection threshold of $F_x(0.5 - 2.0 \text{ keV}) = 3 \times 10^{-14} \text{ erg cm}^2 \text{ s}^{-1}$, comparable to the limit reached in existing deep surveys, as well as the threshold in the all-sky survey proposed to the Dark Energy Task Force (Haiman et al. 2005). In our fiducial model, this yields a cluster surface density of $\sim 5.5 \text{ deg}^{-2}$. Including scatter in the mass-observable relation increases the total number of clusters by $\sim 10\%$ due to preferential upscattering of a larger population of less massive clusters, particularly at high redshift as the mass function steepens. We furthermore impose a strict luminosity floor of $L_{fl} = 3 \times 10^{42} \text{ erg s}^{-1}$ in the observed band, roughly corresponding to the luminosity of small groups (Arnaud & Evrard 1999), below which both observations and our physical model become unreliable. The logarithmic slope of the fiducial mass vs. X-ray luminosity relation is set to $\beta_x = 1.807$ to match the observed scaling, with no evolution $\gamma_x = 0$ (Wang et al. 2004), and a normalization $\log A_x = -3.56$. This then also matches the cluster surface density predicted in the fiducial physical model, and facilitates a fair comparison of the two approaches.

The mock SZ survey is modeled after upcoming observations by the South Pole Telescope (Ruhl et al. 2004; Wang et al. 2004), with a limiting SZ flux of $S_\nu = 3.0 \text{ mJy}$ at $\nu = 150 \text{ GHz}$. This flux threshold produces a yield that again matches the cluster counts of 5.5 deg^{-2} in the mock X-ray survey, allowing an easy comparison. The fiducial power-law parameters are chosen - as before - to match the local scalings with no evolution ($\beta_{sz} = 1.68$ with $\gamma_{sz} = 0$), and the normalization is chosen to agree with the number of clusters predicted by the physical model ($\log A_{sz} = 8.29$).

In both surveys, and for both the physical and phenomenological model, we consider three cases: (1) a single flux bin extending from the detection threshold up to arbitrarily high fluxes, (2) 20 flux bins with no scatter, and (3) 20 flux bins with a log-normal scatter that has a fiducial value of $\sigma_{\log M|\Psi} = 0.1$ for both the X-ray and SZ mass-observable relation (Lima & Hu 2005), but is assumed to be a free parameter. For each of these, we consider two different descriptions of the entropy injection history. First, we fit a power-law evolution of the entropy floor of the form $K_0(z) = K_0(z=0)(1+z)^{\alpha_K}$, with K_0 and α_K as free parameters. Second, we consider arbitrary evolution of the entropy floor K_0 , in which K_0 is fit independently in each of 40 redshift bins of width $\Delta z = 0.05$. In both of these cases, the fiducial entropy floor is set to $K_0 = 125h^{1/3} \text{ keV cm}^2$ with no evolution. For reference, in Figure 6 we show the redshift evolution of $dN/dz d\Omega$ and the of the mass M_{th} corresponding to the detection threshold in both the X-ray and SZ surveys, each for the case of no scatter and $\sigma_{\log M|\Psi} = 0.1$. Finally, for the purpose of comparison, the sky coverage in both surveys is taken to be $\Delta\Omega = 4000 \text{ deg}^2$, the size planned for SPT (Ruhl et al. 2004). For surveys covering a different solid angle, the constraints we obtain below scale as $\propto \Delta\Omega^{-1/2}$.

5.2. CMB Anisotropies

Our simulated CMB survey is modeled after a near to medium-term space based all-sky CMB survey, similar to the proposed Planck mission with bands at 100, 143, and 217 GHz. We assume fractional sky coverage of $f_{sky} \approx 0.8$, and perfect subtraction of foregrounds. The C_ℓ coefficients are calculated up to $\ell_{max} = 2 \times 10^3$ using KINKFAST (Corasaniti et al. 2004), a version of CMB-FAST (Seljak & Zaldarriaga 1996) modified to include a time varying w . See, e.g., Wang et al. (2004) for more details.

6. THE FISHER MATRIX FORECASTS

6.1. Background

With a fiducial cosmology and a prescription for simulating galaxy surveys, one can compute lower limits on statistical errors achievable on model and cosmological parameters. In our self-calibrating approach, the cluster observations are used to simultaneously constrain both the cosmology and model parameters.

Assuming a reasonably well-behaved likelihood function \mathcal{L} , the Fisher matrix is a quick method to forecast joint parameter uncertainties in a multi-parameter fit (Tegmark, Taylor, & Heavens 1997). The Fisher matrix is defined as

$$F_{\alpha\beta} = \left\langle -\frac{\partial^2 \log \mathcal{L}}{\partial p_\alpha \partial p_\beta} \right\rangle \quad (28)$$

where p_α and p_β are free parameters. The inverse of the Fisher matrix gives the best attainable covariance matrix C . Therefore, the constraints on any parameter p_δ , marginalized over all other parameters, is

$$\Delta p_\delta^2 = C_{\delta\delta} = [F^{-1}]_{\delta\delta} \quad (29)$$

We further define a degeneracy coefficient ξ_δ , which quantifies the degree to which degeneracies among the parameters increase the marginalized parameter error over the single-parameter error,

$$\xi_\delta^2 = C_{\delta\delta} F_{\delta\delta}. \quad (30)$$

The degeneracy coefficient ξ_δ ranges from 1 for a purely non-degenerate matrix, to ∞ for fully degenerate parameters.

The combined Fisher matrix for a series of N separate experiments is the sum of the individual Fisher matrices, i.e.

$$F_{tot} = \sum_{i=1}^N F_i \quad (31)$$

which motivates the definition of a synergy coefficient ζ_δ , to quantify the fractional improvement in the marginalized error on a parameter p_δ after combining experiments versus adding the individual experiment errors in quadrature, as

$$\zeta_\delta^2 = C_{\delta\delta} \sum_{i=1}^N ([C_i]_{\delta\delta})^{-1} \quad (32)$$

The synergy coefficient ranges from 1 for no improvement from combining the experiments beyond adding the individual constraints in quadrature, to 0 if the degeneracies are fully broken, in the limiting case that the combined Fisher matrix delivers a perfect knowledge of p_δ .

6.2. Galaxy Cluster Counts

The Fisher matrix for a mock cluster survey, $F_{\alpha\beta}^c$, can be calculated from the number counts of clusters as a function of the observable Ψ . We define the counts Fisher matrix as

$$F_{\alpha\beta}^c = \sum_i \frac{\partial N_i}{\partial p_\alpha} \frac{\partial N_i}{\partial p_\beta} \frac{1}{N_i} \quad (33)$$

where i is the bin index, and the error is purely Poisson counting error (ignoring the modest increase due to sample variance, Hu & Kravtsov (2003)). This represents a sum of several Fisher matrices, one for each independent flux and/or redshift bin.

Therefore, given redshift information, it is possible to derive cosmological constraints from a combination of the flux distribution and redshift evolution of cluster counts. We bin the data by flux - as before - and redshift, giving a Fisher matrix

$$F_{\alpha\beta}^{cz} = \sum_i \sum_j \frac{\partial N_i(z_j)}{\partial p_\alpha} \frac{\partial N_i(z_j)}{\partial p_\beta} \frac{1}{N_i(z_j)} \quad (34)$$

where the sum is taken out to a limiting redshift of z_f . The first $n_{bin} - 1$ flux bins are spaced evenly in log-space from the limiting flux over five orders of magnitude, with a final bin extending out to ∞ . We vary all the cosmological and model parameters, with the exception of $\Omega_b h^2$ and n_s , which are later included via CMB observations. Finally, surveys in different observables are not assumed to overlap.

6.3. CMB Observations

In addition to constraints from cluster counts, we calculated the Fisher matrix for observations of CMB temperature and polarization anisotropies. We assume a Planck-like satellite mission² including both the temperature T and E -mode polarization auto-correlation, as well as the TE cross-correlation, while neglecting B -mode polarization. The full CMB Fisher matrix is then calculated as in Zaldarriaga, Spergel, & Seljak (1997). Each frequency channel was assumed to provide independent cosmological constraints. See Wang et al. (2004) for full details.

7. RESULTS AND DISCUSSION

In order to present our results more clearly, we will proceed in pedagogical order, considering successively more realistic assumptions.

7.1. Cosmology-Only Constraints

In this subsection, we study the limiting case in which the cluster model parameters are known perfectly. We begin with the most naïve experiment, using a single flux bin (i.e. only total cluster counts above the detection threshold, as a function of redshift), and ignoring any scatter in the mass-observable relations. The constraints on the cosmology along with their associated degeneracy coefficients for X-ray and SZ surveys, and the synergy coefficient for the combination are presented in Table 1. The physical model breaks many cosmological degeneracies, and therefore gives much better constraints, for the

X-ray and SZ surveys individually as compared to the phenomenological model. This is particularly true of the dark energy equation of state parameters w_0 and w_a , which improve by a factor of ~ 2 in the X-ray and ~ 4 in the SZ survey. The single parameter sensitivities – the diagonal elements of the Fisher matrix – for w_0 and w_a are comparable in both approaches (physical or phenomenological model). We find that the degeneracy breaking in the physical model is due to better absolute sensitivity to $\Omega_m h^2$. This is because changing $\Omega_m h^2$ while holding $\Omega_b h^2$ fixed (and assuming a flat universe) changes the mean universal baryon fraction. Accordingly, the value of the observables for a cluster of fixed mass will vary with $\Omega_m h^2$. As a result, changes in $\Omega_m h^2$ manifest themselves strongly in the redshift distribution of cluster counts in a flux-limited survey, even at fixed $\Omega_b h^2$, when the physical, rather than phenomenological model, is used to calculate the threshold mass. This difference should be robust, in the sense that any physical model of cluster structure is likely to predict $\Omega_m h^2$ -dependence of the X-ray flux and SZ decrement (over and above the $\Omega_m h^2$ dependence contained in the Hubble parameter $E(z)$ in the power-law relations in equations 21 and 24).

While using the physical model significantly improves the degeneracy coefficients for cosmological parameters in both the X-ray and SZ survey, it also removes the synergy between the two, and degrades the synergy coefficient for their combination. For example, $\zeta_{w_0} \sim 0.60$ for the phenomenological model, as compared to $\zeta_{w_0} \sim 1$ for the physical model. We illustrate this effect by showing the marginalized constraints in the $\Omega_m h^2 - \Omega_{DE}$ plane in Figure 7. The error ellipses shown for phenomenological model (right panel) are larger than for the physical model (left panel), and they are also more complementary, with major axes pointing in different directions. The overall constraints on the cosmology are, however, are still better when the physical models are used.

We next present constraints using 20 flux bins for both the X-ray and SZ surveys in Table 2. Using multiple bins allows additional information to be extracted from the shape of the cluster mass function. As a result, the degeneracy coefficients for all parameters are substantially reduced in both surveys. In fact, all parameters become nearly non-degenerate, and the synergy coefficients in both surveys using either the phenomenological or physical model are close to ~ 1 . Therefore, these constraints reflect the individual parameter sensitivities of the surveys. These sensitivities are roughly equal in the two approaches for all parameters, with the exception of $\Omega_m h^2$, to which the physical model is a factor of ~ 6 more sensitive. This is not surprising, since the cosmological dependence of the physical model reduces to that of the phenomenological model in the limit of $K_0 \sim 0$, expect for the $\Omega_m h^2$ dependence. We therefore confirm our interpretation of constraints using 1 flux bin, and illustrates quantitatively the power of the model to resolve $\Omega_m h^2$. This sensitivity, under more realistic assumptions, will help the physical model break more degeneracies than the phenomenological model.

Constraints for more realistic surveys, in which scatter in the mass-observable relation will degrade the information that can be extracted from the mass-function shape, are summarized in Table 3. These use 20 flux bins in both

² see www.rssd.esa.int/index.php?project=Planck.

the X-ray and SZ, but also include a log-normal scatter as a free parameter. The scatter smears out the shape of the mass function, and increases the degeneracy coefficients for all parameters and in both surveys, to values comparable to those using a single flux bin and no scatter. Overall, the constraints are within a factor of two of the 1-bin, no-scaner case, indicating that scatter destroyed most of the information from the mass function shape. The phenomenological case still has higher overall degeneracy coefficients, which makes the X-ray and SZ constraints more synergistic in combination. On the other hand, the absolute constraints for all parameters are better when the physical model is used.

We also find that imposing priors on the scatter does not significantly improve constraints on the cosmology. This contrasts with the results of Lima & Hu (2005). They, however, use a fixed mass threshold. For a flux limited survey, constraints on the cosmology degrade when a log-normal scatter is introduced as a free parameter, not primarily because of degeneracies among the scatter and the cosmology, but rather because the scatter itself washes out the cosmological sensitivity of the mass-observable relation. To test this hypothesis, we consider constraints on the cosmology and scatter using a fixed mass threshold versus a fixed flux threshold, both with 1 bin. We find that when a fixed mass threshold is used, fixing the scatter improves cosmological constraints by a factor of 2 in most cases, and up a factor of 4 in some. However, when a fixed flux threshold is used, the improvement is typically no more than 30%. This implies that the mass-observable relation, which is flattened by the inclusion of scatter, is driving the constraints on the cosmology.

In summary, for the idealized case when the cluster structure or mass-observable relation is assumed to have no uncertainty, we find that the physical model leads to better sensitivity to dark energy parameters in both the SZ and X-ray surveys individually, and also in the case when the two surveys are combined. We find that this improvement arises because the physical model predicts an increased sensitivity of the observables to $\Omega_m h^2$, which removes degeneracies between $\Omega_m h^2$ and dark energy parameters. Interestingly, the degeneracies are improved so substantially in the individual surveys, that the combination of the two surveys is *less* synergistic than in the phenomenological case.

7.2. Self-Calibrated Constraints

In this subsection, we present self-calibrated constraints, in which the parameters of the phenomenological or physical model, are assumed to be a-priori unknown. We will focus on the extent to which this degrades cosmological constraints. It is worth noting, however, that such a self-calibration approach can yield tight constraint not just on the cosmology, but also on the properties of the clusters themselves.

In Table 4, we show self-calibrated constraints in the simplest case of 1 flux bin with no scatter. The results show that the phenomenological model parameters are extremely degenerate with the cosmology, suggesting their ability to introduce changes in dN/dz in ways that mimic the effects of changing the cosmology. This has been noted previously: for example, uncertainties in the normalization of the observed mass-temperature

relation result in large uncertainties in the value of σ_8 measurements (Seljak 2002; Pierpaoli et al. 2003) when this value is inferred from the cluster temperature function. The severe degeneracies between cosmological and mass-observable relation parameters are manifest in the high values of the degeneracy parameters, especially for σ_8 , with of $\xi_{\sigma_8} \sim 100$ and 600 for the X-ray and SZ surveys respectively. When the X-ray and SZ surveys are combined, it is possible to break some of these degeneracies, but for σ_8 , and for the dark energy parameters in particular, the synergy coefficients $\zeta_{w_0, w_a} \sim 1$, indicating that uncertainty in the slope, normalization, or evolution of the mass-observable relations in the X-ray or SZ can mimic the effects of variations in these cosmological parameters.

The above contrasts sharply with the results we obtain using a physical model – as the bottom half of Table 4 shows, there is only minor degradation of the cosmological parameter constraints due to the uncertainties in f_g , K_0 , and α_K . In this case, the X-ray parameter degeneracies on average increase only by a factor of $\sim 2 - 3$ as compared to the case of perfect knowledge of the model parameters, while the SZ degeneracies increase by no more than 40%. This demonstrates that the physical model parameters f_g , K_0 , and α_K do not easily mimic the effects of a change in cosmology. The comparison with the phenomenological model is especially dramatic for the dark energy equation of state parameters in the SZ survey, whose constraints are improved by a factor of ~ 10 . In addition, because these parameters simultaneously determine both the X-ray and SZ mass-observable relations, and because they enter into the expressions for the flux differently (through ρ_g^2 for the X-ray and ρ_g for the SZ flux), the two surveys are more complementary than in the case when these parameters are fixed. Therefore, the synergy coefficients are smaller than their analogues in Table 1.

In Table 5, we extract information from the shape of the mass function, by using 20 flux bins, while still assuming no scatter in the mass-observable relation. As before, we find that the shape of the mass function helps to break many of the parameter degeneracies, with $\xi \sim 1 - 2$ for all parameters, and thus these constraints again are indicative of the single parameter sensitivities. In the middle and the bottom set of rows in this table, we consider two different parametrizations of the entropy injection history in the physical model: power-law, and arbitrary evolution of K_0 with redshift. In both cases, the degeneracy coefficients for all parameters are significantly lower than those in the direct self-calibration models. They are somewhat higher for arbitrary K_0 -evolution by a factor of ~ 1.5 , indicating that relaxing the assumption of a power-law evolution can better mimic the effects of dark energy. However, in this case of arbitrary K_0 evolution, the X-ray and SZ constraints are more synergistic in combination. Therefore, when both the X-ray and SZ results are considered, the absolute parameter constraints are degraded by no more than $\sim 20 - 30\%$ even when K_0 can evolve arbitrarily with redshift. We also see, as in the previous section, far greater sensitivity to $\Omega_m h^2$ when using the physical rather than the phenomenological model.

Finally, the constraints in the most realistic among our

mock surveys, which includes 20 flux bins and a log-normal scatter as a free parameter, is presented in Table 6. As we found in the the cosmology-only constraints above, the uncertainty in the scatter increases the degeneracies for all parameters, in both surveys, and for both the phenomenological and physical model results. For the phenomenological model, we recover the complementarity of the two surveys. However, both cases of the physical model give smaller degeneracy coefficients and better absolute constraints for all parameters. In particular, using the physical model improves w_0 and w_a constraints by a factor of 2 relative to the phenomenological model. We also note that allowing arbitrary K_0 -evolution still does not significantly degrade constraints, even in the presence of uncertain scatter, relative to a power-law K_0 -evolution. Interestingly, we find that this is because for a physical model with arbitrary K_0 evolution, the X-ray and SZ surveys are exceptionally complementary. In particular, the synergy coefficient for the dark energy parameters $\zeta_{w_0, w_a} < 0.7$, indicating that constraints improve by more than 30% (over adding the constraints in quadrature) when the X-ray and SZ surveys are combined. This is illustrated visually in Figure 8, where we show marginalized constraints in the $w_0 - w_a$ plane. The figure shows a significant reduction in the size of the error ellipse when the two surveys are combined. In particular, this reduction is much more significant in the physical model (left panel) than in the case of the phenomenological model (right panel).

7.3. Complementary Observations

Finally, we contrast the constraints we find from the mock cluster surveys to measurement of CMB anisotropies (by Planck). The constraints and degeneracy coefficients we find for Planck individually are listed in Table 7. The table shows that the forecasts for the combined X-ray and SZ cluster surveys, even when we allow for unknown scatter, and for arbitrary entropy-injection history, compares favorably with Planck, including $\Omega_m h^2$ which is known to be measured to exquisite precision with the CMB.

We also investigate the utility of CMB measurements in breaking the parameter degeneracies inherent in the X-ray and SZ cluster surveys. Constraints for the combination of Planck with the X-ray and SZ cluster surveys (including 20 bins and uncertain scatter, as in Table 6) are listed in Table 8. The inclusion of the Planck data adds substantial sensitivity to the individual parameters, which results in a significant increase in the degeneracy coefficients. We find that when Planck data is assumed to be available, the combination of X-ray and SZ data, using a phenomenological model, is not particularly synergistic. All the synergy coefficients $\zeta(CMB + XR + SZ) > 0.75$, with constraints on the dark energy equation of state unimproved relative to adding the three individual experiment errors in quadrature. This implies that CMB observations resolve the degeneracies that were previously broken by the combination of X-ray and SZ data. This is also the case for a physical model with power-law K_0 evolution. However, for arbitrary K_0 evolution, we still find significant improvement in constraints for the combination of X-ray and SZ data, even in the presence of CMB data, with $\zeta(CMB + XR + SZ) < 0.8$ for all parameters, and

$\zeta(CMB + XR + SZ) \sim 0.7$ for dark energy equation of state parameters. This degeneracy breaking is only slightly weaker than in the absence of CMB data. Indeed, though the addition of Planck data to the individual surveys yields noticeably improved constraints on dark energy, when is included in the combined surveys it helps little with the w_0 and w_a constraints, since their marginalized uncertainties are dominated by the degeneracies that remain with the cluster model parameters (rather than among cosmological parameters).

8. SENSITIVITY TO THE ADOPTED PHYSICAL MODEL

While the above results are promising, one may worry that they rely on the specific choice for the underlying physical model. In particular, if real data is fit with the wrong model, the derived cosmological parameters may suffer from a bias larger than their uncertainty we inferred above. Such potential biases could be directly quantified by creating mock data using various “true” models, and obtaining the best-fit to these data using different, parameterized, “wrong” models. The magnitude of the bias, in general, will depend strongly on the pair of models that are compared – and hence, ultimately, on which way the real data falls. A full exploration of these biases also requires going beyond the Fisher matrix approach adopted here, and will be postponed to a future paper.

Nevertheless, one can use the Fisher approach to quantify the impact of wrong model assumptions, by adding new degrees of freedom, representing uncertainties about the underlying physical model, and evaluating the degradation in the statistical errors. This degradation can be regarded as the systematic error arising from the choice of the wrong model, among a restricted set of possible models.

Specifically, here we allow the gas fraction to evolve as $f_g \sim (1+z)^{\alpha_{f_g}}$, and the entropy injection to vary with mass as $K_0 \sim M^{\kappa_M}$ and radius as $K_0 \sim (1+x)^{\kappa_x}$. To maintain our rough agreement with observations, the fiducial model is chosen to match that used for the previous analysis, with $\alpha_{f_g} = \kappa_M = \kappa_x = 0$, and the three additional parameters included in our self-calibrated Fisher forecasts for a power-law evolving entropy injection with 20 flux bins and a log-normal scatter.

We then compute the constraints for cosmological parameters as before, to see the extended to which they are degraded by the addition of these new degrees of freedom. We find that in the X-ray survey, the cosmological parameter constraints degrade by about a factor of ~ 2 , while in the SZ survey, the constraints degrade by no more than 15%. This behavior is to be expected, as the X-ray luminosity scales as $\sim \rho_g^2$, as compared to the SZ luminosity that scales as ρ_g , and is therefore more sensitive to changes in the physical model. Likewise, the model parameter constraints degrade by $\sim 60\%$ in both the X-ray and SZ surveys. When both surveys are combined, the cosmological parameter constraints degrade by no more than $\sim 20\% - \lesssim 10\%$ for the dark energy equation of state – while the model parameter constraints degrade by $\sim 50\%$. At the same time, we are able to constrain α_{f_g} – the evolution of the gas fraction – to within 0.14 and 0.11 from the X-ray and SZ surveys individually, and 0.06 from their combination; roughly similar to constraints on the evolution of the entropy injection.

Likewise, we are able to constrain the values of the new parameters to within ~ 0.02 from the X-ray and SZ surveys individually, and 0.01 from the combination.

Therefore, we conclude that the greatest impact of introducing additional flexibility to the model is to degrade theoretical constraints on the model parameters themselves. The cosmological constraints, particularly for the SZ and combined surveys, are more robust to relaxing the model assumptions. Using a model with three extra degrees of freedom, even in the case of the X-ray survey, which is particularly sensitive to the model behavior, the theoretical constraints using a physical model are substantially better than those using a phenomenological fit. While these results are encouraging, a more complete treatment, allowing for a wider range of (non-power-law) models, would be necessary to estimate possible systematic errors.

9. FUTURE WORK

Though these results above are promising, we here note some important reservations. Firstly, the goal in our study is to motivate a methodology, rather than a specific cluster structure model. We believe that the improvement in the constraints in individual experiments arises because adopting a physical model introduces new cosmology sensitivity that is not present when the mass-observable relation is parametrized directly. For the preheated model we consider here, the dominant effect is the new $\Omega_m h^2$ -sensitivity, which we expect to hold generically, regardless of the details of a cluster model. Likewise, the improvement in the synergy between the SZ and X-ray surveys arises because the physical model relates the X-ray flux and the SZ decrement (one cannot be changed without changing the other). This, again, should be a generic feature of any model that directly models the ICM gas distribution. A caveat to this last conclusion is that the model may have uncertainties, such as gas clumping or a strong radial dependence of the entropy injection $K_0(r)$, which will change the X-ray flux relative to the SZ decrement, which will tend to reduce the synergy between the two surveys.

Nevertheless, before fits to real data can be performed, there is significant work to be done in modeling cluster structure and evolution more accurately. Modified entropy models, though very successful at predicting mass-observable relations and their evolution, are incorrect in detail (Pratt & Arnaud 2005; Pratt, Arnaud, & Pointecouteau 2006). We also find some tension between our model predictions and observed local scaling relations and number counts (see Figures 3, and 5). Furthermore, in addition to having models that fit cluster structure data accurately, one has to also know the correct cosmological dependence of the observables in these models. In the future, we envision that three-dimensional simulations, including the relevant non-gravitational and gas physics, at least in parametrized manner, and also including asymmetries in cluster structure, as well as deviations from hydrostatic

equilibrium, will provide such models.

In addition to an improved model of cluster structure, more realistic constraints require a detailed treatment of the systematics of any real survey. Our work represents a “best case scenario”, in which the X-ray and SZ surveys are idealized in many ways. With the introduction of scatter, and using bin sizes far wider than any reasonable observational error on flux measurements, the inclusion of systematic uncertainties in flux measurements will not significantly change our overall results. On the other hand, completeness and selection issues will degrade final errors, and may effect the complementarity we have found. As large-scale cluster surveys start taking data, a more thorough understanding of the combination of the systematic and statistical uncertainties will be required to interpret our results.

10. CONCLUSIONS

Using a Fisher Matrix approach, we have demonstrated that the use of a physically motivated model of the ICM in mock large-scale cluster surveys gives significantly better constraints on cosmological and model parameters, and better synergy between SZ and X-ray surveys, than one can obtain by directly parametrizing the mass-observable relation. In particular, when both the cosmology and model parameters are included in the fit, for the simplest case of pure cluster counts as a function of redshift (see Table 4), the physical model yields constraints on the dark energy equation of state that are 2 times tighter and 3 times less degenerate in the X-ray, and 10 times tighter and 15 times less degenerate in the SZ than those using a phenomenological model. If the shape of the mass function and scatter in the mass-observable relation are included and the entropy floor is taken to be an arbitrary function of redshift (see Table 6), the dark energy parameter constraints are 20% times tighter and 2 times less degenerate in the X-ray, and 2 times tighter and 2 times less degenerate in the SZ than those using a phenomenological model. In addition, these constraints are up to a factor of two tighter than those from simply adding the individual experiment errors in quadrature, relative to a minor 20% improvement from combining constraints using a phenomenological model. These results suggest that parametrized physical models of cluster structure will be useful when extracting constraints on both cosmology, and cluster structure itself, from future large-scale SZ and X-ray cluster surveys.

We thank Justin Khoury for providing the Planck Fisher matrix, and the referee for many helpful comments. This work was supported in part by NSF grant AST-05-07161, by the U.S. Department of Energy under Contract No. DE-AC02-98CH10886, and by the Columbia University Initiatives in Science and Engineering (ISE) funds. Greg Bryan acknowledges support from NSF grant AST-0547823.

REFERENCES

- Arnaud, M. & Evrard, A. E., 1999, MNRAS, 305, 631
 Bahcall, N. A. & Bode, P., 2003, ApJ, 588, L1
 Bahcall, N. A. & Cen, R., 1992, ApJ, 398, L81
 Bahcall, N., et al., 2003, ApJ, 585, 182
 Bahcall, N. A., 1988, ARA&A, 26, 63
 Blake, C. & Glazebrook, K., 2003, ApJ, 594, 665
 Borgani, S., et al., 2001, ApJ, 561, 13

- Brown, M. L., Taylor, A. N., Bacon, D. J., Gray, M. E., Dye, S., Meisenheimer, K., & Wolf, C., 2003, *MNRAS*, 341, 100
- Bullock, J. S., Kolatt, T. S., Sigad, Y., Somerville, R. S., Kravtsov, A. V., Klypin, A. A., Primack, J. R., & Dekel, A., 2001, *MNRAS*, 321, 559
- Chevallier, M. & Polarski, D., 2001, *Int. J. Mod. Phys. D10*, 213
- Carlberg, R. G., Morris, S. L., Yee, H. K. C., & Ellingson, E., 1997, *ApJ*, 479, L19
- Corasaniti, P. S., Kunz, M., Parkinson, D., Copeland, E. J., & Bassett, B. A., 2004, *Phys. Rev. D*, 70, 083006
- Eisenstein, D. J. & Hu, W., 1999, *ApJ*, 511, 5
- Eke, V. R., Navarro, J. F., & Steinmetz, M., 2001, *ApJ*, 554, 114
- Fairley, B. W., Jones, L. R., Scharf, C., Ebeling, H., Perlman, E., Horner, D., Wegner, G., & Malkan, M., 2000, *MNRAS*, 315, 669
- Finoguenov, A., Reiprich, T. H., & Böhringer, H. 2001, *A&A*, 368, 749
- Fixsen, D. J., et al., 1996, *ApJ*, 473, 576
- Freese, K., Adams, F. C., & Frieman, J. A., 1987, *Nucl. Phys. B*, 298, 797
- Giavalisco, M., et al., 2004, *ApJ*, 600, L103
- Gioia, I. M., Henry, J. P., Mullis, C. R., Voges, W., Briel, U. G., Böhringer, H., & Huchra, J. P., 2001, *ApJ*, 533, L105
- Girardi, M., Giuricin, G., Mardirossian, F., Mezzetti, M., & Boschin, W., 1998, *ApJ*, 505, 74
- Gladders, M. D., Yee, H. K. C., Majumdar, S., Barrientos, L. F., Hoekstra, H., Hall, P. B., & Infante, L., *astro-ph/0603588*
- Haiman, Z., et al., 2005, *astro-ph/0507013*
- Haiman, Z., Mohr, J. J., & Holder, G. P., 2001, *ApJ*, 553, 545
- Helsdon, S. F. & Ponman, T. J., 2000, *MNRAS*, 319, 933
- Henry, J. P. & Arnaud, K. A., 1991, *ApJ*, 372, 410
- Henry, J. P., 2004, *ApJ*, 609, 603
- Hoekstra, H., van Waerbeke, L., Gladders, M. D., Mellier, Y. & Yee, H. K. C., 2002, *ApJ*, 577, 604
- Holder, G. P., Haiman, Z., & Mohr, J. J., 2001, *ApJ*, 560, L111
- Horner, D. J., Mushotzky, R. F. & Scharf, C. A., 1999, *ApJ*, 520, 78
- Hu, W. & Haiman, Z., 2003, *Phys. Rev. D*, 68, 3004
- Hu, W. & Kravtsov, A. V., 2003, *ApJ*, 584, 702
- Hu, W., 2003, *Phys. Rev. D*, 67, 081304
- see Jahoda, K., 2003, *Astronomische Nachrichten*, 324, 132
- Jarvis, M., Bernstein, G. M., Fischer, P., Jain, B., Tyson, J. A., & Wittman, D., 2003, *AJ*, 125, 1014
- Jenkins, A., Frenk, C. S., White, S. D. M., Colberg, J. M., Cole, S., Evrard, A. E., Couchman, H. M. P., & Yoshida, N., 2001, *MNRAS*, 321, 372
- Kuhlen, M., Strigari, L., Zetnet, A., Bullock, J., & Primack, J., 2005, *MNRAS*, 357, 387
- Levine, E. S., Schultz, A. E., & White, M., 2002, *ApJ*, 577, 569
- Lima, M. & Hu, W., 2005, *Phys. Rev. D*, 72, 043006
- Linder, E. V., 2003, *Phys. Rev. D*, 68, 3504
- Lloyd-Davies, E. J., Ponman, T. J., & Cannon, D. B., 2000, *MNRAS*, 315, 689
- Majumdar, S. & Mohr, J. J., 2004, *ApJ*, 613, 41
- Markevich, M., 1998, *ApJ*, 504, 27
- Maughan, B. J., Jones, L. R., Ebeling, H., & Scharf, C., 2005, *MNRAS*, 365, 509
- McCarthy, I. G., Babul, A., Holder, G. P., & Balogh, M. L., 2003a, 591, 515
- McCarthy, I. G., Babul, A., Holder, G. P., & Balogh, M. L., 2003b, 591, 526
- Navarro, J. F., Frenk, C. S. & White, S. D. M., 1997, *ApJ*, 490, 493
- Novicki, M. C., Sornig, M. A., & Henry, J. P., 2002, *ApJ*, 123, 2413
- Peebles, P. J. E., 1993, *Principles of Physical Cosmology* (Princeton Univ. Press)
- Peebles, P. J. E., Daly, R. A., & Juskiewicz, R., 1989, *ApJ*, 347, 563
- Pierpaoli, E., Borgani, S., Scott, D., & White, M., 2003, *MNRAS*, 342, 163
- Pointecouteau, E., Arnaud, M., Kaastra, J., & de Plaa, J., 2004, *A&A*, 423, 33
- Ponman, T. J., Cannon, D. B., & Navarro, J. F., 1999, *Nature*, 397, 135
- Pratt, G. W. & Arnaud, M., 2005, *A&A*, 429, 791
- Pratt, G. W., Arnaud, M., & Pointecouteau, E., 2006, *A&A*, 446, 429
- Press, W. H. & Schechter, P. I., 1974, *ApJ*, 187, 425
- Raymond, J. C. & Smith, B. W., 1977, *ApJS*, 35, 419
- Refregier, A., Valtchanov, I., & Pierre, M., 2002, *A&A*, 390, 1
- Reiprich, T. & Böhringer, H., 2002, *ApJ*, 567, 716
- Rosati, P., Borgani, S., & Norman, C., 2002, *ARA&A*, 40, 539
- see Ruhl, J., et al., 2004, *Proc. SPIE*, 5498, 11
- Sanderson, A. J. R., Ponman, T. J., Finoguenov, A., Lloyd-Davies, E. J., & Marketich, M., 2003, *MNRAS*, 340, 989
- Seljak, U. & Zaldarringo, M., 1996, *ApJ*, 469, 437
- Seljak, U., 2002, *MNRAS*, 337, 769
- Seo, H.-J. & Eisenstein, D. J., 2003, *ApJ*, 598, 720
- Shuecker, P., Böhringer, H., Collins, C. A., & Guzzo, L., 2003, *A&A*, 298, 867
- Spergel, D.N., Verde, L., Peiris, H.V. Komatsu, E., Nolta, M.R., Bennett, C.L., Halpern, M., Hinshaw, G., Jarosik, N., Kogut, A., Limon, M. Meyer, S.S., Page, L., Tucker, G.S., Weiland, J.L., Wollack, E., & Wright, E.L., 2003, *ApJS*, 148, 175
- Spergel, D. N., Bean, R., Dore, O., Nolta, M. R., Bennett, C. L., Hinshaw, G., Jarosik, N., Komatsu, E., Page, L., Peiris, H. V., Verde, L., Barnes, C., Halpern, M., Hill, R. S., Kogut, A., Limon, M., Meyer, S. S., Odegard, N., Tucker, G. S., Weiland, J. L., Wollack, E., & Wright, E. L., *ApJ*, submitted, *astro-ph/0603449*
- Sun, M., Jones, C., Murray, S. S., Allen, S. W., Fabian, A. C., & Edge, A. C., 2003, *ApJ*, 587, 619
- Sunyaev, R. & Zeldovich, Y., 1972, *Comments Astrophys. Space Phys.*, 2, 66
- Sunyaev, R. & Zeldovich, Y., 1980, *MNRAS*, 190, 413
- Tegmark, M., Taylor, A. N., & Heavens, A. F., 1997, *ApJ*, 480, 22
- Tyson, A. J., et al., 2002, *Proc. SPIE Int. Soc. Opt. Eng.* 4836, pp. 10–20, *astro-ph/0302102* (see also www.lsst.org)
- Verde, L., Haiman, Z., & Spergel, D., 2002, *ApJ*, 581, 5
- Viana, P. P. & Liddle, A. R., 1996, *MNRAS*, 262, 1023
- Vikhlinin, A., McNamara, B. R., Forman, W., Jones, C., Quintana, H., & Hornstrup, A., 1998, *ApJ*, 502, 558
- Vikhlinin, A., Markevitch, M., Murray, S. S., Jones, C., Forman, W., & Van Speybroeck, L., 2004, *ApJ*, 628, 655
- Voit, M. G., Bryan, G. L., Balogh, M. L., & Bower, R. G., 2002, *ApJ*, 576, 601
- Wang, S., Khoury, J., Haiman, Z., & May, M., 2004, *Phys. Rev. D*, 70, 7013008
- Well, J. & Battye, R. A., 2003, *New Astronomy Reviews*, 47, 775
- Weller, J., Battye, R. A., & Kneissl, R., 2002, *Phys. Rev. Lett.*, 88, 1301
- White, D. A., Jones, C., & Forman, W., 1997, *MNRAS*, 292, 419
- Willick, J. A. & Strauss, M. A., 1998, *ApJ*, 507, 64
- Xu, H., Jin, G & Wu, X.-P. 2001, *ApJ*, 553, 78
- Younger, J. D. & Bryan, G. L., in preparation
- Zaldarriaga, M., Spergel, D. N., & Seljak, U., 1997, *ApJ*, 488, 1

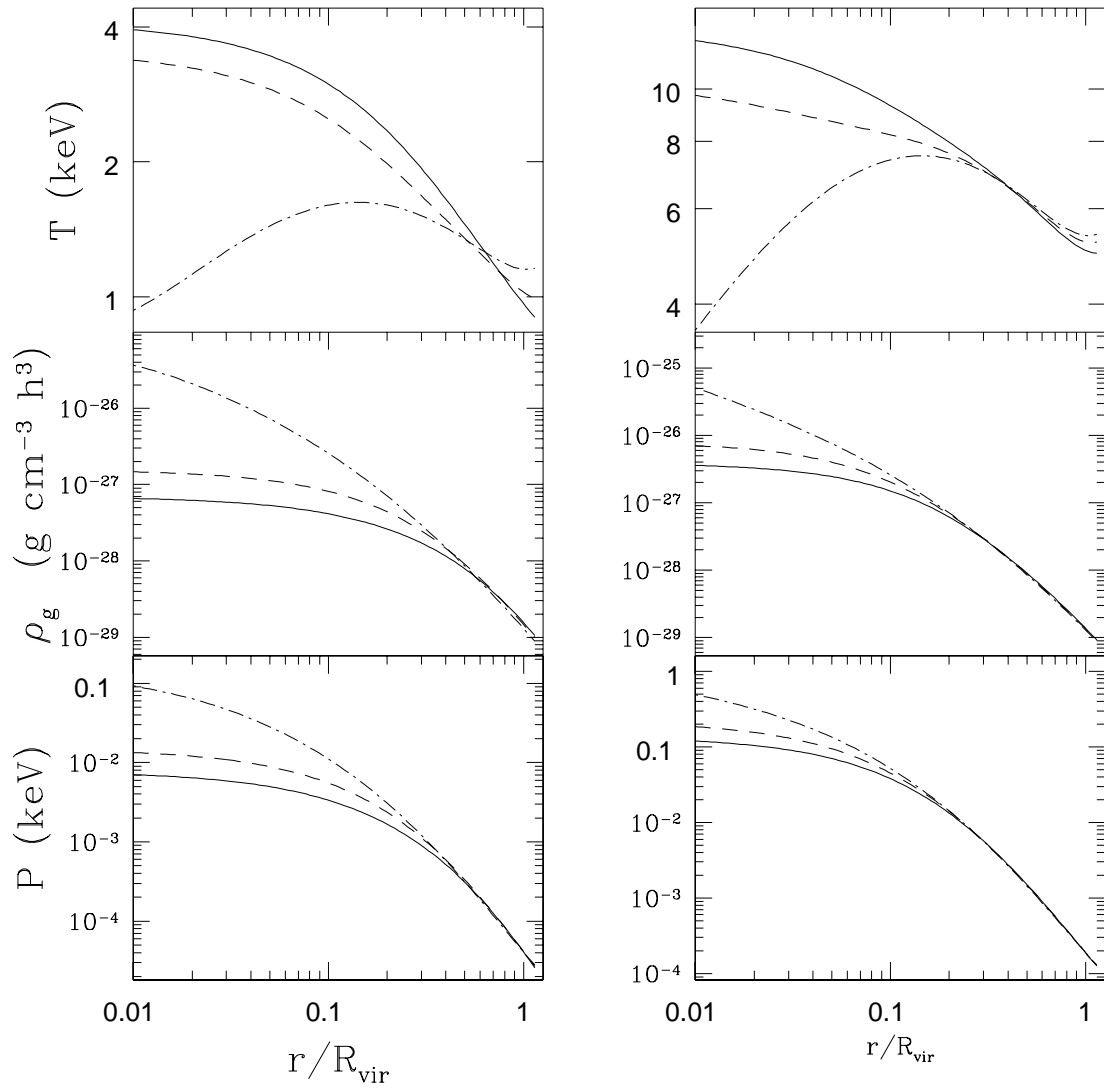


FIG. 1.— The pressure, density, and temperature profiles for a cluster with a total (gas + DM) mass of $10^{14} h^{-1} M_{\odot}$ (left panels) and $10^{15} h^{-1} M_{\odot}$ (right panels). The profiles are computed at redshift $z = 0$, assuming that the intra-cluster gas is in hydrostatic equilibrium in an NFW halo. The three curves in each panel correspond to different amounts of preheating: $K_0 = 0$ (no preheating; dash-dotted curves), $K_0 = 50$ (dashed curves), and 100 keV cm^2 (solid curves; close to our fiducial choice of $125 h^{1/3} \text{ keV cm}^2$).

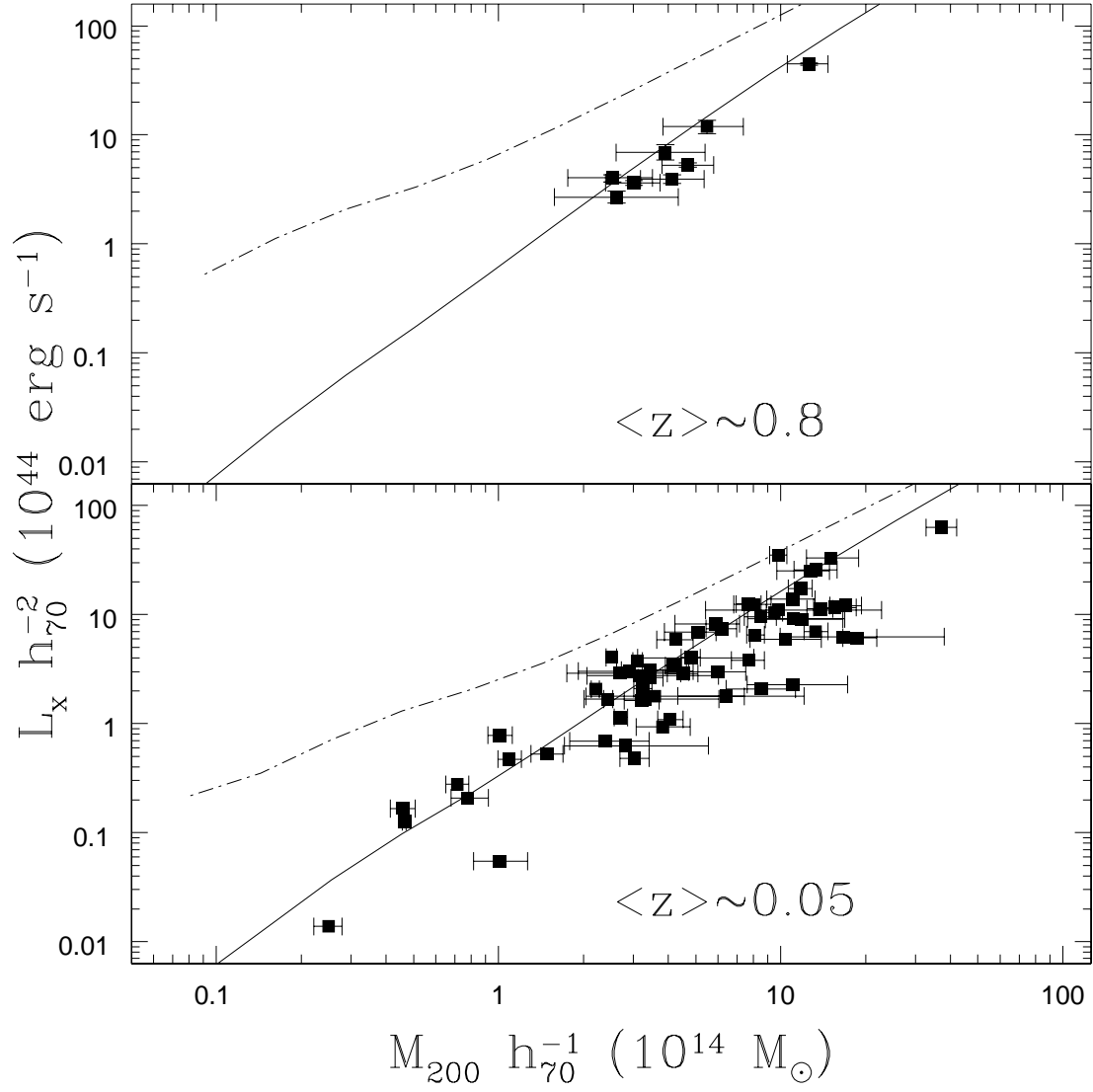


FIG. 2.— The local (bottom panel) and high-redshift (top panel) mass-luminosity relation between mass and X-ray luminosity for the self-similar model without preheating (dot-dashed curves) and the fiducial model, with a non-evolving entropy floor $K_0 = 125h^{1/3}$ keV cm² (solid curves). The data points show measurements in the range $0 < z < 0.1$ (Reiprich & Böhringer 2002) and $0.7 < z < 0.9$ (Maughan et al. 2005). The model predictions are computed at corresponding mean redshifts of $\langle z \rangle = 0.05$ and $\langle z \rangle = 0.8$.

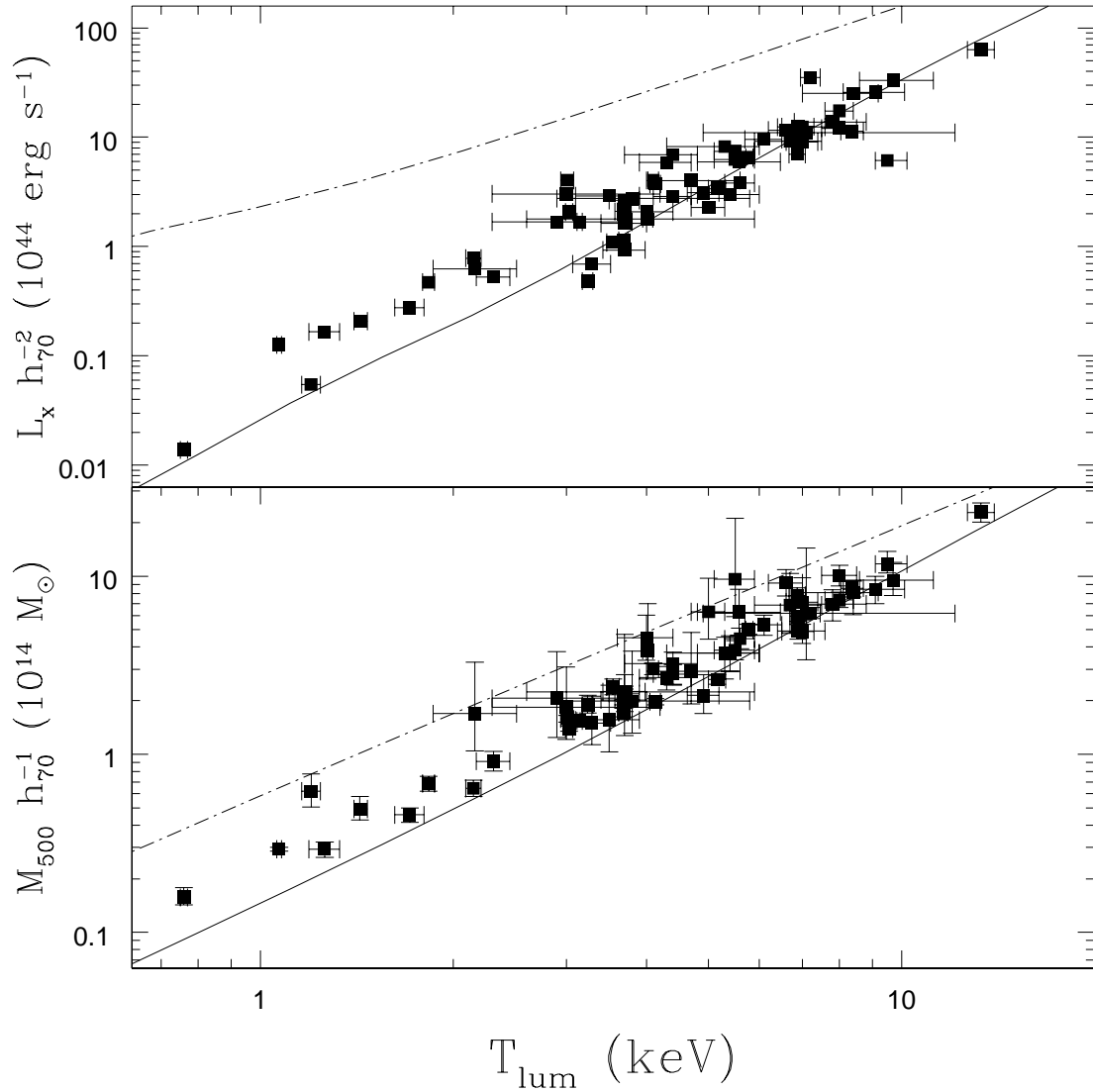


FIG. 3.— The local mass–temperature (bottom panel) and temperature–luminosity (top panel) relations for the self–similar model without preheating (dot–dashed curves) and the fiducial model with a non–evolving entropy floor $K_0 = 125h^{1/3}$ keV cm² (solid curves). The data points are from local measurements at $0 < z < 0.1$ (Reiprich & Böhringer 2002), and the model predictions are computed at the corresponding mean redshift of $\langle z \rangle = 0.05$.

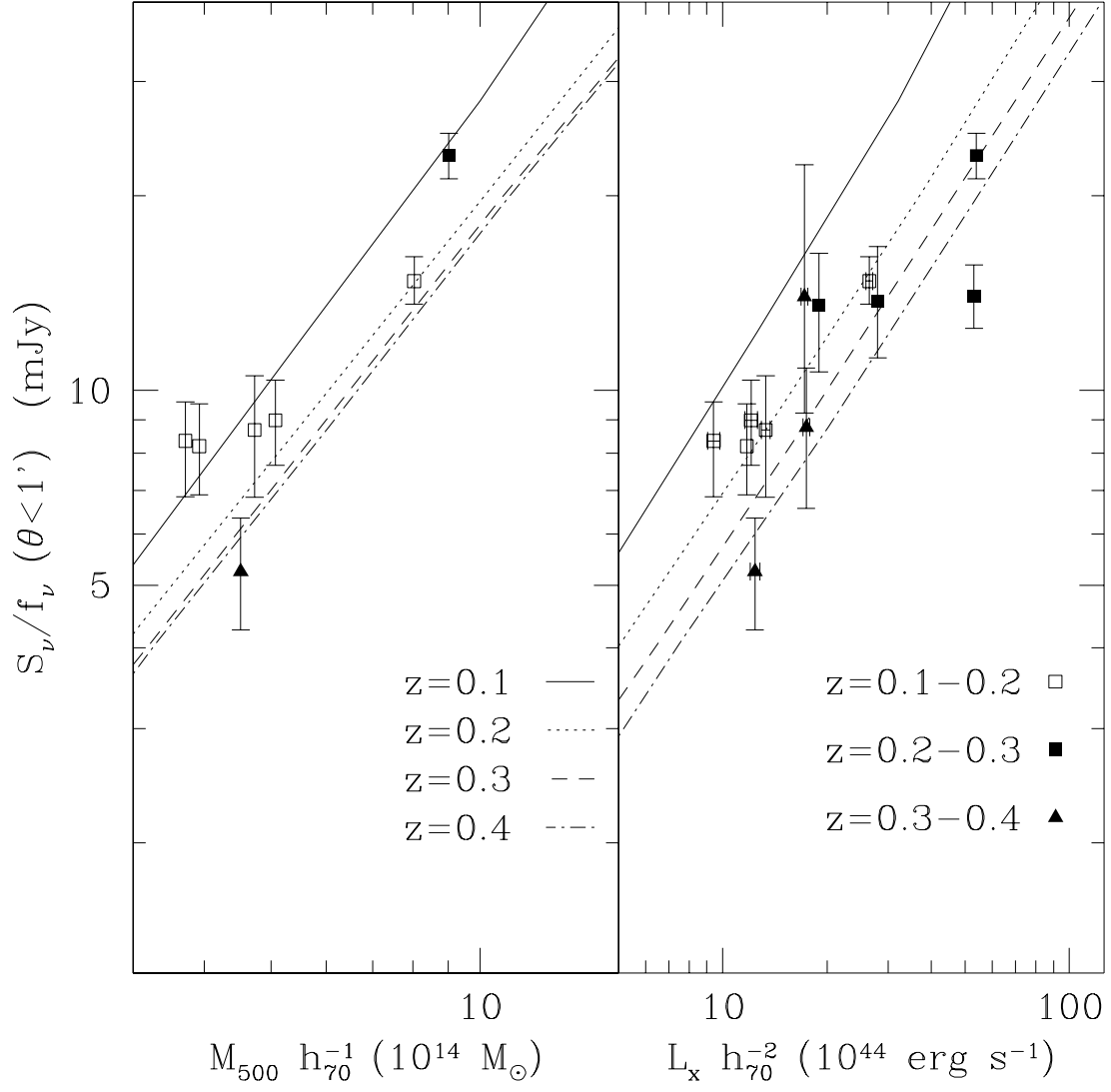


FIG. 4.— Model predictions at four different redshifts in the range $0 < z < 0.4$ for scaling relations involving the SZ flux, in the fiducial model with a non-evolving entropy floor of $K_0 = 125h^{1/3} \text{ keV cm}^2$. The data points with errors, shown in three different redshift bins, are taken from McCarthy et al. (2003a) and references therein.

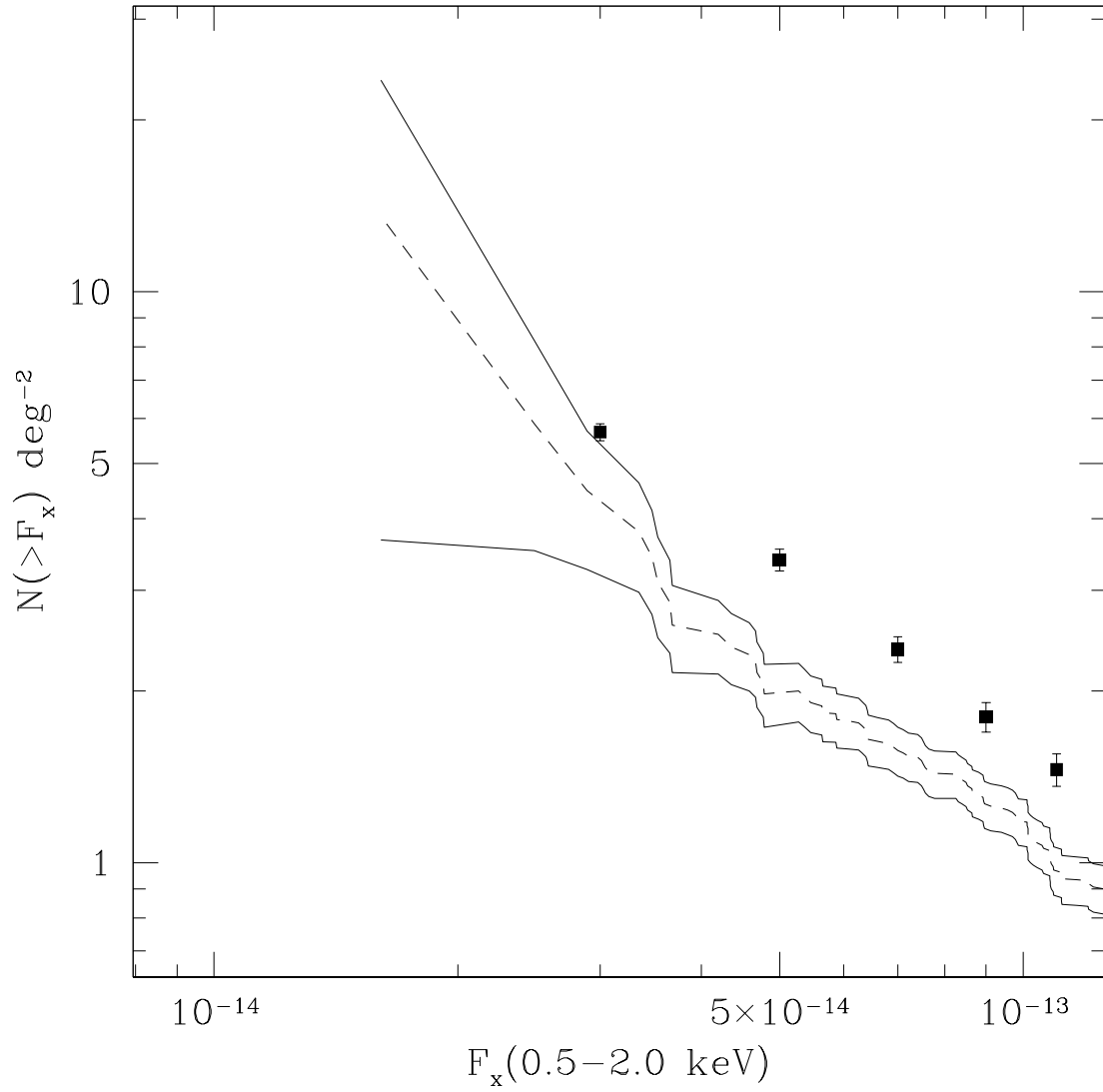


FIG. 5.— The cumulative X-ray source counts predicted in our fiducial model, as a function of soft X-ray flux in the 0.5-2.0 keV band, compared to observations by Vikhlinin et al. (1998) (dashed curve) bracketed by corresponding 1σ error bars (solid curves). The fiducial model predictions are shown as filled squares with Poisson error bars. At the flux limit of $F_x > 3 \times 10^{-14} \text{ erg s}^{-1}$ used in our analysis, we find a source density of 5.5 deg^{-2} , in agreement with observations, while at higher fluxes, the model somewhat overpredicts the number of clusters.

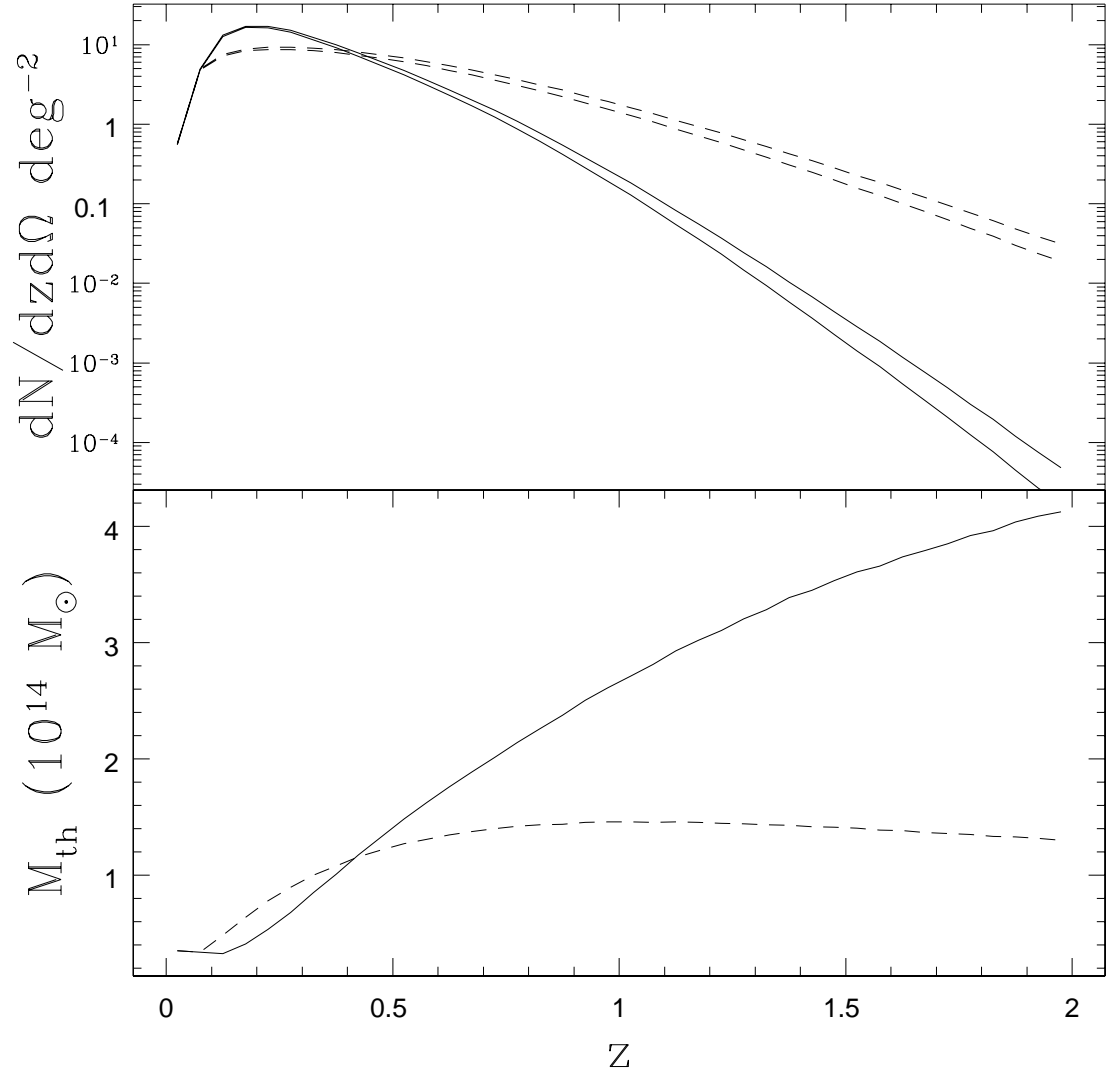


FIG. 6.— The lower panel shows the evolution of the limiting mass M_{th} corresponding to the flux detection threshold, and the upper panel shows the number counts of clusters above this mass, in the mock X-ray (solid curves) and SZ (dashed curves) surveys. The pairs of curves in the top panel correspond to the case of no scatter in the mass-observable relation (lower curve) and a log-normal scatter in the mass, at fixed observable, of $\sigma_{\log M|\Psi} = 0.1$ (upper curve).

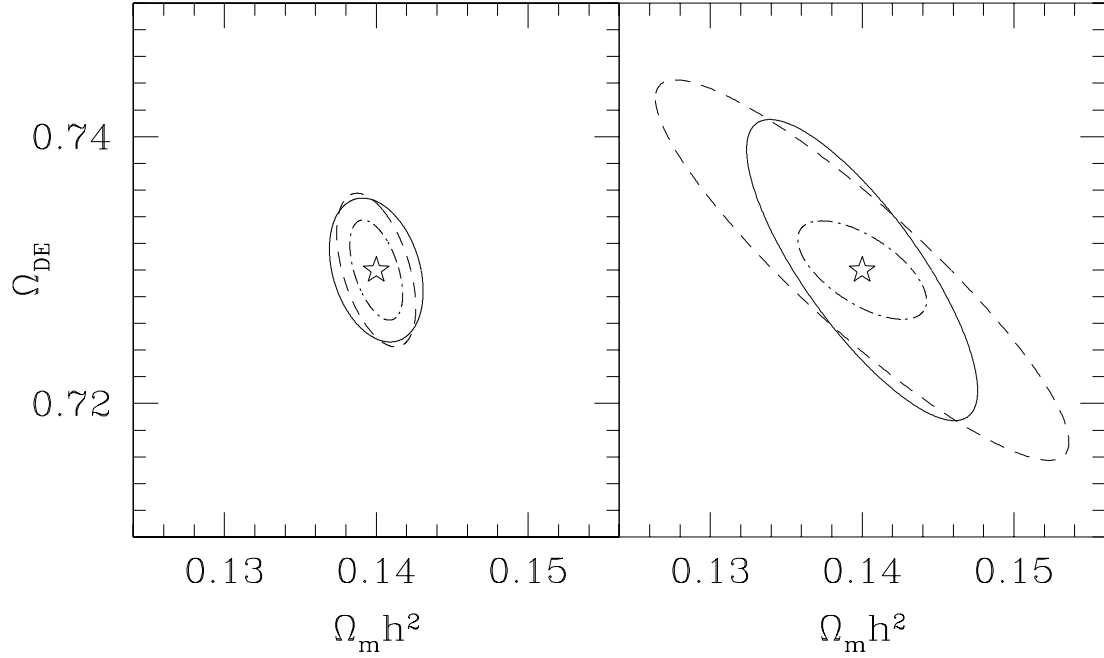


FIG. 7.— Parameter constraints in the $\Omega_m h^2 - \Omega_{DE}$ plane for direct self-calibration of the mass-observable relation (right panel) and using the physical model (left panel). The constraints have been marginalized over all other cosmological parameters. The figure assumes a single flux bin (the shape of the mass function is not used) and no scatter in the mass-observable relation (see Table 1). In both panels, we show constraints from the mock X-ray (solid ellipses) and SZ (dashed ellipses) surveys individually, and from the combination of the two surveys (dot-dashed ellipses). Note the overall improvement in the constraints when the physical model is used, arising from breaking the $w - \Omega_m h^2$ degeneracies within each survey.

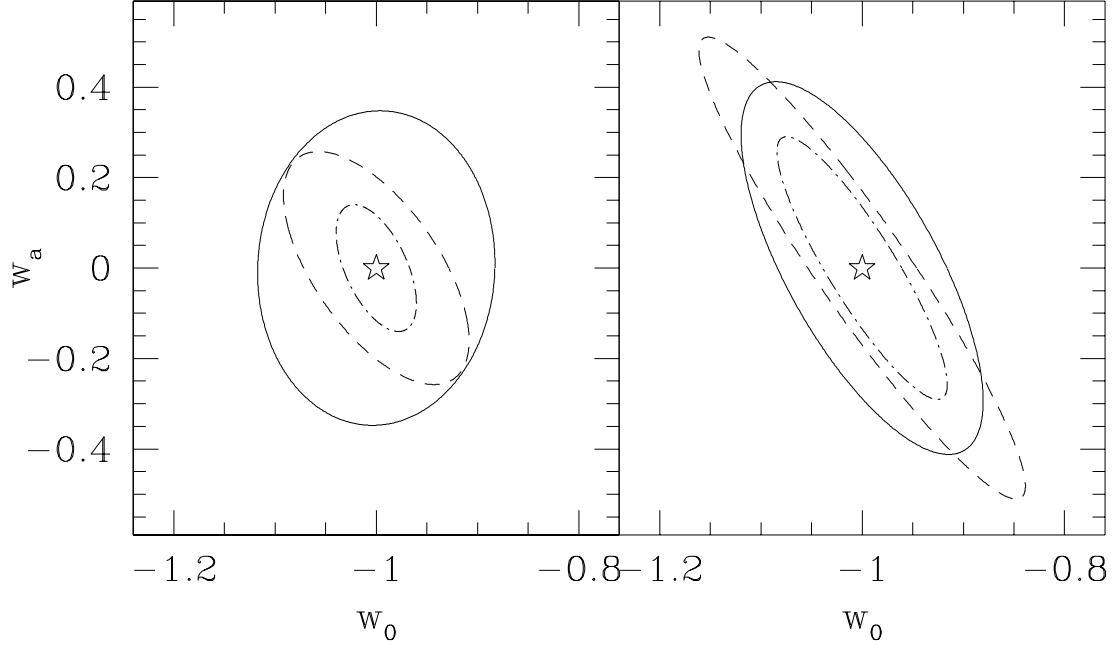


FIG. 8.— Parameter constraints in the $w_0 - w_a$ plane for direct self-calibration of the mass-observable relation (right panel) and using the physical model (left panel). The constraints have been marginalized over all other cosmological parameters. The figure assumes $n_{bin} = 20$ independent flux bins, and a log-normal scatter in the mass-observable relation that is a priori unknown (with the fiducial value of $\sigma_{\log M|\Psi} = 0.1$; see Table 6). In both panels, we show constraints from the mock X-ray (solid ellipses) and SZ (dashed ellipses) surveys individually, and from the combination of the two surveys (dot-dashed ellipses). Note the improved degeneracy breaking in the physical model, when data from the two surveys are combined.

TABLE 1
COSMOLOGICAL CLUSTER CONSTRAINTS FOR $n_{bin} = 1$ AND NO SCATTER

		$\Delta p(XR)$	$\xi(XR)$	$\Delta p(SZ)$	$\xi(SZ)$	$\Delta p(XR + SZ)$	$\zeta(XR + SZ)$
Phenomenological Model	$\Delta\Omega_m h^2$	5.01×10^{-3}	2.4	8.98×10^{-3}	4.9	2.80×10^{-3}	0.64
	$\Delta\Omega_{DE}$	7.44×10^{-3}	10	9.40×10^{-3}	11	2.43×10^{-3}	0.42
	Δw_0	0.10	9.0	0.17	17	5.14×10^{-2}	0.59
	Δw_a	0.31	5.5	0.57	11	0.21	0.78
	$\Delta\sigma_8$	1.31×10^{-2}	15	1.31×10^{-2}	19	3.69×10^{-3}	0.40
Physical Model	$\Delta\Omega_m h^2$	2.67×10^{-3}	1.6	2.10×10^{-3}	3.0	1.40×10^{-3}	0.85
	$\Delta\Omega_{DE}$	4.68×10^{-3}	4.0	4.25×10^{-3}	5.5	3.04×10^{-3}	0.97
	Δw_0	4.90×10^{-2}	2.9	3.35×10^{-2}	3.0	2.64×10^{-2}	0.96
	Δw_a	0.19	1.8	9.89×10^{-2}	1.8	8.34×10^{-2}	0.96
	$\Delta\sigma_8$	4.33×10^{-3}	4.5	3.98×10^{-3}	5.6	2.75×10^{-3}	0.94

TABLE 2
COSMOLOGICAL CLUSTER CONSTRAINTS FOR $n_{bin} = 20$ AND NO SCATTER

		$\Delta p(XR)$	$\xi(XR)$	$\Delta p(SZ)$	$\xi(SZ)$	$\Delta p(XR + SZ)$	$\zeta(XR + SZ)$
Phenomenological Model	$\Delta\Omega_m h^2$	7.08×10^{-4}	1.1	1.22×10^{-3}	1.3	6.06×10^{-4}	0.99
	$\Delta\Omega_{DE}$	8.07×10^{-4}	1.5	1.15×10^{-3}	1.8	6.32×10^{-4}	0.96
	Δw_0	6.85×10^{-3}	1.2	7.27×10^{-3}	1.3	4.89×10^{-3}	0.98
	Δw_a	6.45×10^{-3}	1.0	9.05×10^{-3}	1.2	5.07×10^{-3}	0.97
	$\Delta\sigma_8$	1.31×10^{-3}	1.6	1.28×10^{-3}	1.9	8.49×10^{-4}	0.93
Physical Model	$\Delta\Omega_m h^2$	1.44×10^{-4}	1.0	2.01×10^{-4}	1.1	1.17×10^{-4}	0.99
	$\Delta\Omega_{DE}$	7.10×10^{-4}	1.1	6.15×10^{-4}	1.3	4.53×10^{-4}	0.98
	Δw_0	9.21×10^{-3}	1.1	1.01×10^{-2}	1.2	6.61×10^{-3}	0.97
	Δw_a	1.22×10^{-2}	1.1	9.55×10^{-3}	1.1	7.20×10^{-3}	0.96
	$\Delta\sigma_8$	1.06×10^{-3}	1.2	1.06×10^{-3}	1.5	7.01×10^{-4}	0.93

TABLE 3
COSMOLOGICAL CLUSTER CONSTRAINTS FOR $n_{bin} = 20$ AND $\sigma_{\log M|\Psi} = 0.1$ LOG-NORMAL SCATTER

		$\Delta p(XR)$	$\xi(XR)$	$\Delta p(SZ)$	$\xi(SZ)$	$\Delta p(XR + SZ)$	$\zeta(XR + SZ)$
Phenomenological	$\Delta\Omega_m h^2$	1.94×10^{-3}	2.3	5.08×10^{-3}	3.7	1.31×10^{-3}	0.72
	$\Delta\Omega_{DE}$	4.23×10^{-3}	6.5	7.21×10^{-3}	9.1	2.07×10^{-3}	0.57
	Δw_0	6.21×10^{-2}	6.0	9.15×10^{-2}	10	3.94×10^{-2}	0.77
	Δw_a	0.23	4.2	0.32	6.7	0.16	0.86
	$\Delta\sigma_8$	7.26×10^{-3}	9.0	8.57×10^{-3}	13	2.83×10^{-3}	0.51
	$\Delta\sigma_{XR}$	1.22×10^{-3}	1.20×10^{-3}	...
	$\Delta\sigma_{SZ}$	5.73×10^{-3}	...	3.11×10^{-3}	...
Physical Model	$\Delta\Omega_m h^2$	1.55×10^{-3}	1.6	1.51×10^{-3}	2.3	9.99×10^{-4}	0.92
	$\Delta\Omega_{DE}$	2.75×10^{-3}	2.7	3.81×10^{-3}	5.1	2.11×10^{-3}	0.95
	Δw_0	3.62×10^{-2}	2.5	3.01×10^{-2}	3.0	2.02×10^{-2}	0.87
	Δw_a	0.12	1.5	9.38×10^{-2}	1.8	7.16×10^{-2}	0.96
	$\Delta\sigma_8$	8.01×10^{-3}	8.7	4.19×10^{-3}	6.1	2.39×10^{-3}	0.64
	$\Delta\sigma_{XR}$	1.61×10^{-2}	9.90×10^{-3}	...
	$\Delta\sigma_{SZ}$	2.45×10^{-2}	...	1.4	...

TABLE 4
 SELF-CALIBRATED CLUSTER CONSTRAINTS FOR $n_{bin} = 1$ WITH NO SCATTER .

		$\Delta p(XR)$	$\xi(XR)$	$\Delta p(SZ)$	$\xi(SZ)$	$\Delta p(XR + SZ)$	$\zeta(XR + SZ)$	
Phenomenological Model	$\Delta\Omega_m h^2$	2.73×10^{-2}	13	0.15	82	1.18×10^{-2}	0.44	
	$\Delta\Omega_{DE}$	5.97×10^{-2}	85	0.17	206	2.19×10^{-2}	0.39	
	Δw_0	0.21	18	0.50	50	0.15	0.80	
	Δw_a	0.32	5.7	1.1	21	0.27	0.88	
	$\Delta\sigma_8$	8.31×10^{-2}	98	0.43	627	5.51×10^{-2}	0.67	
	$\Delta \log A_x$	0.26	0.23	...	
	$\Delta\beta_x$	0.21	0.15	...	
	$\Delta\gamma_x$	0.64	0.41	...	
	$\Delta \log A_{sz}$	1.3	...	0.14	...	
	$\Delta\beta_{sz}$	0.83	...	0.10	...	
	$\Delta\gamma_{sz}$	2.1	...	0.53	...	
	Physical Model $K_0(z) = K_0(1+z)^{\alpha_K}$	$\Delta\Omega_m h^2$	4.01×10^{-3}	2.3	2.18×10^{-3}	3.1	1.66×10^{-3}	0.87
		$\Delta\Omega_{DE}$	1.37×10^{-2}	11	4.65×10^{-3}	6.1	3.63×10^{-3}	0.82
Δw_0		0.12	7.0	3.39×10^{-2}	3.1	2.84×10^{-2}	0.87	
Δw_a		0.19	1.8	0.10	1.8	8.54×10^{-2}	0.96	
$\Delta\sigma_8$		2.01×10^{-2}	20	5.77×10^{-3}	8.1	4.28×10^{-3}	0.77	
Δf_g		7.07×10^{-2}	...	3.76×10^{-2}	...	2.25×10^{-2}	...	
ΔK_0		18	...	6.2	...	3.0	...	
$\Delta\alpha_K$		0.36	...	0.10	...	6.03×10^{-2}	...	

TABLE 5
 SELF-CALIBRATED CLUSTER CONSTRAINTS FOR $n_{bin} = 20$ WITH NO SCATTER.

		$\Delta p(XR)$	$\xi(XR)$	$\Delta p(SZ)$	$\xi(SZ)$	$\Delta p(XR + SZ)$	$\zeta(XR + SZ)$	
Phenomenological Model	$\Delta\Omega_m h^2$	7.36×10^{-4}	1.2	1.78×10^{-3}	1.9	6.53×10^{-4}	0.96	
	$\Delta\Omega_{DE}$	8.64×10^{-4}	1.6	1.22×10^{-3}	1.9	6.74×10^{-4}	0.96	
	Δw_0	7.19×10^{-3}	1.3	8.03×10^{-3}	1.4	5.28×10^{-3}	0.99	
	Δw_a	6.53×10^{-3}	1.0	9.31×10^{-3}	1.2	5.16×10^{-3}	0.96	
	$\Delta\sigma_8$	1.76×10^{-3}	2.2	2.13×10^{-3}	3.2	1.30×10^{-3}	0.96	
	$\Delta \log A_x$	1.89×10^{-3}	1.74×10^{-3}	...	
	$\Delta\beta_x$	3.42×10^{-3}	2.95×10^{-3}	...	
	$\Delta\gamma_x$	9.23×10^{-4}	9.01×10^{-4}	...	
	$\Delta \log A_{sz}$	4.08×10^{-3}	...	3.20×10^{-3}	...	
	$\Delta\beta_{sz}$	5.69×10^{-3}	...	4.39×10^{-3}	...	
	$\Delta\gamma_{sz}$	5.07×10^{-4}	...	4.81×10^{-4}	...	
	Physical Model $K_0(z) = K_0(1+z)^{\alpha_K}$	$\Delta\Omega_m h^2$	1.48×10^{-4}	1.1	2.08×10^{-4}	1.1	1.17×10^{-4}	0.98
		$\Delta\Omega_{DE}$	7.40×10^{-4}	1.1	6.16×10^{-4}	1.3	4.59×10^{-4}	0.97
Δw_0		1.00×10^{-2}	1.2	1.05×10^{-2}	1.3	6.87×10^{-3}	0.95	
Δw_a		1.23×10^{-2}	1.1	1.05×10^{-2}	1.2	7.46×10^{-3}	0.93	
$\Delta\sigma_8$		1.88×10^{-3}	2.0	1.21×10^{-3}	1.7	8.63×10^{-4}	0.85	
Δf_g		4.18×10^{-3}	...	3.60×10^{-3}	...	2.48×10^{-3}	...	
ΔK_0		0.74	...	0.91	...	0.52	...	
$\Delta\alpha_K$		2.19×10^{-2}	...	1.64×10^{-2}	...	1.15×10^{-2}	...	
Physical Model Arbitrary $K_0(z)$		$\Delta\Omega_m h^2$	1.95×10^{-4}	1.4	2.53×10^{-4}	1.3	1.32×10^{-4}	0.86
	$\Delta\Omega_{DE}$	8.34×10^{-4}	1.3	8.69×10^{-4}	1.9	4.90×10^{-4}	0.81	
	Δw_0	1.15×10^{-2}	1.4	1.37×10^{-2}	1.7	8.08×10^{-3}	0.91	
	Δw_a	1.62×10^{-2}	1.4	1.48×10^{-2}	1.6	8.68×10^{-3}	0.79	
	$\Delta\sigma_8$	2.08×10^{-3}	2.3	1.62×10^{-3}	2.3	9.82×10^{-4}	0.77	
	Δf_g	4.48×10^{-3}	...	4.10×10^{-3}	...	2.70×10^{-3}	...	
	$\langle \Delta K_0 \rangle$	1.3	...	1.2	...	0.68	...	

TABLE 6
 SELF-CALIBRATED CLUSTER CONSTRAINTS FOR $n_{bin} = 20$ AND $\sigma_{\log M|\Psi} = 0.1$ LOG-NORMAL SCATTER.

		$\Delta p(XR)$	$\xi(XR)$	$\Delta p(SZ)$	$\xi(SZ)$	$\Delta p(XR + SZ)$	$\zeta(XR + SZ)$
Phenomenological	$\Delta\Omega_m h^2$	5.93×10^{-3}	6.9	2.89×10^{-2}	21	2.58×10^{-3}	0.44
	$\Delta\Omega_{DE}$	1.43×10^{-2}	22	1.32×10^{-2}	16	5.66×10^{-3}	0.58
	Δw_0	7.88×10^{-2}	7.7	0.11	11	5.55×10^{-2}	0.88
	Δw_a	0.27	4.9	0.34	7.1	0.19	0.91
	$\Delta\sigma_8$	1.40×10^{-2}	17	1.56×10^{-2}	23	8.85×10^{-3}	0.85
	$\Delta \log A_x$	2.56×10^{-2}	1.72×10^{-2}	...
	$\Delta\beta_x$	2.09×10^{-2}	1.22×10^{-2}	...
	$\Delta\gamma_x$	9.67×10^{-2}	5.80×10^{-2}	...
	$\Delta\sigma_{XR}$	1.24×10^{-3}	1.23×10^{-3}	...
	$\Delta \log A_{sz}$	3.20×10^{-2}	...	2.12×10^{-2}	...
	$\Delta\beta_{sz}$	4.77×10^{-2}	...	1.36×10^{-2}	...
	$\Delta\gamma_{sz}$	3.32×10^{-2}	...	2.80×10^{-2}	...
	$\Delta\sigma_{SZ}$	6.25×10^{-3}	...	5.71×10^{-3}	...
	Physical Model $K_0(z) = K_0(1+z)^{\alpha_K}$	$\Delta\Omega_m h^2$	1.66×10^{-3}	1.7	1.55×10^{-3}	2.4	1.05×10^{-3}
$\Delta\Omega_{DE}$		2.86×10^{-3}	2.8	4.11×10^{-3}	5.5	2.22×10^{-3}	0.95
Δw_0		5.18×10^{-2}	3.5	3.03×10^{-2}	3.0	2.16×10^{-2}	0.83
Δw_a		0.13	1.5	9.60×10^{-2}	1.9	7.30×10^{-2}	0.95
$\Delta\sigma_8$		9.40×10^{-3}	10	5.31×10^{-3}	7.8	3.33×10^{-3}	0.72
$\Delta\sigma_{XR}$		6.47×10^{-3}	4.89×10^{-3}	...
$\Delta\sigma_{SZ}$		7.55×10^{-3}	...	6.30×10^{-3}	...
Δf_g		2.09×10^{-2}	...	2.67×10^{-2}	...	1.10×10^{-2}	...
ΔK_0		5.0	...	3.8	...	2.2	...
$\Delta\alpha_K$		8.79×10^{-2}	...	7.65×10^{-2}	...	4.37×10^{-2}	...
Physical Model Arbitrary $K_0(z)$		$\Delta\Omega_m h^2$	2.12×10^{-3}	2.1	2.17×10^{-3}	3.3	1.19×10^{-3}
	$\Delta\Omega_{DE}$	3.66×10^{-3}	3.6	7.11×10^{-3}	9.6	2.56×10^{-3}	0.79
	Δw_0	7.73×10^{-2}	5.2	6.05×10^{-2}	5.9	2.61×10^{-2}	0.55
	Δw_a	0.23	2.7	0.17	3.3	9.25×10^{-2}	0.68
	$\Delta\sigma_8$	1.45×10^{-2}	15	7.85×10^{-3}	11	3.62×10^{-3}	0.52
	$\Delta\sigma_{XR}$	7.79×10^{-3}	5.61×10^{-3}	...
	$\Delta\sigma_{SZ}$	9.77×10^{-3}	...	6.74×10^{-3}	...
	Δf_g	2.48×10^{-2}	...	3.94×10^{-2}	...	1.23×10^{-2}	...
	$\langle \Delta K_0 \rangle$	2.2	...	2.8	...	1.5	...

TABLE 7
 COSMOLOGICAL CONSTRAINTS FOR CMB OBSERVATIONS.

	$\Delta p(PLANCK)$	$\xi(PLANCK)$
$\Delta\Omega_m h^2$	1.21×10^{-3}	23
$\Delta\Omega_{DE}$	3.46×10^{-2}	72
Δw_0	0.32	166
Δw_a	1.04	152
$\Delta\sigma_8$	4.11×10^{-2}	88
$\Delta\Omega_b h^2$	1.36×10^{-4}	...
Δn_s	3.54×10^{-3}	...

TABLE 8
 SELF-CALIBRATED CLUSTER+CMB CONSTRAINTS FOR $n_{bin} = 20$ AND $\sigma_{\log M|\Psi} = 0.1$ LOG-NORMAL SCATTER.

		$\Delta p(XR)$	$\xi(XR)$	$\Delta p(SZ)$	$\xi(SZ)$	$\Delta p(XR + SZ)$	$\zeta(XR + SZ)$	
Power-Law Model	$\Delta\Omega_m h^2$	5.93×10^{-4}	11	5.34×10^{-4}	10	3.35×10^{-4}	0.89	
	$\Delta\Omega_{DE}$	3.17×10^{-3}	8.2	5.53×10^{-3}	13	2.07×10^{-3}	0.76	
	Δw_0	6.07×10^{-2}	32	8.67×10^{-2}	46	4.77×10^{-2}	0.97	
	Δw_a	0.20	30	0.25	37	0.16	1.0	
	$\Delta\sigma_8$	4.87×10^{-3}	12	1.12×10^{-2}	29	3.78×10^{-3}	0.85	
	$\Delta\Omega_b h^2$	1.10×10^{-4}	...	1.11×10^{-4}	...	1.07×10^{-4}	...	
	Δn_s	2.56×10^{-3}	...	2.49×10^{-3}	...	2.30×10^{-3}	...	
	$\Delta \log A_x$	2.21×10^{-2}	1.07×10^{-4}	...	
	$\Delta\beta_x$	9.97×10^{-3}	2.30×10^{-3}	...	
	$\Delta\gamma_x$	4.26×10^{-2}	1.67×10^{-2}	...	
	$\Delta\sigma_{XR}$	1.22×10^{-3}	1.22×10^{-3}	...	
	$\Delta \log A_{sz}$	2.71×10^{-2}	...	1.82×10^{-2}	...	
	$\Delta\beta_{sz}$	1.32×10^{-2}	...	1.22×10^{-2}	...	
	$\Delta\gamma_{sz}$	2.50×10^{-2}	...	2.28×10^{-2}	...	
	$\Delta\sigma_{SZ}$	5.00×10^{-3}	...	4.50×10^{-3}	...	
Physical Model $K_0(z) = K_0(1+z)^{\alpha_K}$	$\Delta\Omega_m h^2$	5.72×10^{-4}	10	3.79×10^{-4}	7.2	2.97×10^{-4}	0.97	
	$\Delta\Omega_{DE}$	2.39×10^{-3}	5.5	3.61×10^{-3}	9.0	1.85×10^{-3}	0.93	
	Δw_0	3.18×10^{-2}	16	2.85×10^{-2}	15	1.98×10^{-2}	0.93	
	Δw_a	0.12	17	8.44×10^{-2}	12	6.67×10^{-2}	0.97	
	$\Delta\sigma_8$	5.91×10^{-3}	14	5.05×10^{-3}	13	3.03×10^{-3}	0.79	
	$\Delta\Omega_b h^2$	1.13×10^{-4}	...	1.05×10^{-4}	...	1.03×10^{-4}	...	
	Δn_s	2.54×10^{-3}	...	2.33×10^{-3}	...	2.26×10^{-3}	...	
	$\Delta\sigma_{XR}$	5.59×10^{-3}	4.74×10^{-3}	...	
	$\Delta\sigma_{SZ}$	6.39×10^{-3}	...	5.26×10^{-3}	...	
	Δf_g	1.37×10^{-2}	...	2.59×10^{-2}	...	1.04×10^{-2}	...	
	ΔK_0	3.4	...	3.7	...	2.1	...	
	$\Delta\alpha_K$	5.02×10^{-2}	...	7.50×10^{-2}	...	3.88×10^{-2}	...	
	Physical Model $K_0(z) = K_0(1+z)^{\alpha_K}$	$\Delta\Omega_m h^2$	6.70×10^{-4}	12	4.96×10^{-4}	9.4	3.04×10^{-4}	0.80
		$\Delta\Omega_{DE}$	2.73×10^{-3}	6.3	6.46×10^{-3}	16	2.08×10^{-3}	0.83
		Δw_0	4.45×10^{-2}	23	5.53×10^{-2}	29	2.38×10^{-2}	0.69
Δw_a		0.18	25	0.15	22	7.98×10^{-2}	0.70	
$\Delta\sigma_8$		7.49×10^{-3}	18	7.44×10^{-3}	19	3.37×10^{-3}	0.64	
$\Delta\Omega_b h^2$		1.16×10^{-4}	...	1.08×10^{-4}	...	1.04×10^{-4}	...	
Δn_s		2.67×10^{-3}	...	2.45×10^{-3}	...	2.27×10^{-3}	...	
$\Delta\sigma_{XR}$		5.3	6.8	...	
$\Delta\sigma_{SZ}$		4.1	...	2.8	...	
Δf_g		7.03×10^{-3}	...	8.33×10^{-3}	...	5.51×10^{-3}	...	
ΔK_0		1.62×10^{-2}	...	3.52×10^{-2}	...	5.81×10^{-3}	...	
$\Delta\alpha_K$		13	...	8.3	...	1.12×10^{-2}	...	